**İSTANBUL TECHNICAL UNIVERSITY ★ INSTITUTE OF SCIENCE AND TECHNOLOGY**

# VORTEX-INDUCED VIBRATIONS OF AN ELASTICALLY MOUNTED CIRCULAR CYLINDER IN TWO DEGREES OF FREEDOM

**M.Sc. Thesis by**

**Salim KOÇ**

**Department : Aeronautical Engineering**

**Programme: Aeronautical Engineering**

**MAY 2002**

**İSTANBUL TECHNICAL UNIVERSITY ★ INSTITUTE OF SCIENCE AND TECHNOLOGY**

# VORTEX-INDUCED VIBRATIONS OF AN ELASTICALLY MOUNTED CIRCULAR CYLINDER IN TWO DEGREES OF FREEDOM

**M.Sc. Thesis by**
**Salim KOÇ**
**(511991032)**

**Date of submission : 13 May 2002**

**Date of defence examination: 31 May 2002**

**Supervisor (Chairman): Prof. Dr. M. Fevzi ÜNAL**

**Members of the Examining Committee: Doç. Dr. Metin Orhan KAYA**

**Yrd. Doç. Dr. N. L .O. Çetiner Yıldırım**

**MAY 2002**

**ACKNOWLEDGEMENTS**

I would like to thank to my supervisor Prof. Dr. M. Fevzi ÜNAL for allowing me to study together on this exciting subject. I gratefully acknowledge his support.

I also appreciate valuable help of Assistant Prof. N. L .O. Çetiner Yıldırım throughout my studies.

Lastly, I would like to thank my family. They have done everything for me. They have supported me to come here. I will never forget their support.

May, 2002 Salim KOÇ

**CONTENTS**

**LIST OF TABLES**

**Page No**

## LIST OF FIGURES

## LIST OF SYMBOLS

| | |
|---|---|
| $\mathbf{c}$ | : Damping constant |
| $\mathbf{C_D}$ | : Drag Coefficient |
| $\mathbf{C_L}$ | : Lift Coefficient |
| $\mathbf{D}$ | : Cylinder diameter |
| $\vec{\mathbf{F}}$ | : Force Vector |
| $\mathbf{f_n}$ | : Natural frequency |
| $\mathbf{f_s^*}$ | : Vortex shedding frequency |
| $\mathbf{f_n^*}$ | : Natural frequency of fluid-structure system |
| $\mathbf{f_s^*}$ | : Vortex shedding frequency of rigid body |
| $\vec{\mathbf{g}}$ | : Gravity vector |
| $\mathbf{J}$ | : Jacobian of the transformation |
| $\mathbf{k}$ | : Spring constant per unit length |
| $\mathbf{M^*}$ | : Mass ratio |
| $\mathbf{m}$ | : Mass |
| $\mathbf{p}$ | : Pressure |
| $\mathbf{R}$ | : Cylinder Radius |
| $\mathbf{Re}$ | : Reynolds number based on D |
| $\mathbf{Sg}$ | : Reduced Damping parameter |
| $\mathbf{T}$ | : Dimensionless time ($t\ U_\infty /D$) |
| $\mathbf{U_\infty}$ | : Free Stream Velocity |
| $\mathbf{t}$ | : Time |
| $\vec{\mathbf{U}}$ | : Velocity vector |
| $\mathbf{V}$ | : Volume |
| $\mathbf{Vr}$ | : Reduced Velocity |
| $\mathbf{X}$ | : Cylinder streamwise displacement |
| $\mathbf{Y}$ | : Cylinder transverse displacement |
| $\mathbf{z}$ | : Physical cylinder plane |
| $\mathbf{\Gamma}$ | : Circulation |
| $\mathbf{\Delta t}$ | : Time step of calculation |
| $\zeta$ | : Computational plane |
| $\mu$ | : Dynamic Viscosity |
| $\rho$ | : Fluid density |
| $\rho_s$ | : Structure density |
| $\tau$ | : Skin friction |
| $\psi$ | : Stream function |
| $\xi_s$ | : Structural damping parameter |
| $\omega$ | : Vorticity |

**VORTEX-INDUCED VIBRATIONS OF AN ELASTICALLY MOUNTED CIRCULAR CYLINDER IN TWO DEGREES OF FREEDOM**

## SUMMARY

Fluid-Structure Interactions occur in many engineering fields. These interactions give rise to complicated vibrations of the structures and can cause structural damage under certain unfavourable conditions. A common fluid-structure interaction problem is the flow-induced vibrations of a structure caused by vortex shedding from the structure. In this study, a numerical study of a uniform flow past an elastically mounted circular cylinder using the discrete vortex method incorporating the vortex in cell (VIC) technique has been undertaken. The Reynolds number based on the cylinder diameter is kept at 200 for all calculations and the cylinder motion is modelled by a spring-damper-mass system. The fluid motion and the structural responses are solved in an iterative way so that the interactions between the fluid and the structure can be accounted for properly.

Analyses of the cylinder responses, the induced forces, the vortex shedding frequency and the vortex structure in the wake have been carried out. In these analyses, effect of structure to fluid density ratio $M^*=m/(\rho D^2)$ (where m is the structural mass, $\rho$ is the fluid density, D is the cylinder diameter) as function of the frequency ratio $f_n/f_s^*$ (where $f_n$ is the structural frequency, $f_s^*$ is the natural vortex shedding frequency of rigid cylinder) is examined for a constant reduced damping parameter Sg=0.01. At a constant Strouhal number, Sg is proportional to multiplication of damping factor with M*.

Five different values of mass parameter M* extending from 1 to 10 are examined. In order to have a significant vortex-induced response, the frequency ratio, fn/fs*, ranges from 0.65 to 2.6, with most of the cases concentrated around fn/fs*=1. Drag, lift coefficients, cylinder oscillations in x and y directions and the variation with time of the corresponding wake structures are examined to find the locking-on region. The results are compared with previous numerical studies. A fair agreement is found.

# İKİ SERBESTLİK DERECELİ, ELASTİK BAĞLI BİR DAİRESEL SİLİNDİRDE VORTEKSLERİN İNDÜKLEDİĞİ TİTREŞİMLER

## ÖZET


Akışkan-Yapı etkileşimlerine çoğu mühendislik alanında rastlanmaktadır. Bu etkileşimler yapının titreşimlerini arttırır ve bazı istenmeyen şartlar altında yapısal hasarlara neden olabilir. Sıklıkla karşılaşılan bir akış-yapı etkileşimi, yapıdan ayrılan vortekslerin yapı üzerinde titreşimler indüklemesi şeklindedir. Bu çalışmada, üniform bir akış alanı içinde iki serbestlik derecesine sahip olacak şekilde elastik olarak bağlı bir dairesel silindirin vortekslerce indüklenen titreşimleri "Vortex in Cell" tekniğini de kapsayan ayrık vorteks metodu ile sayısal olarak incelenmiştir. Tüm hesaplamalarda silindirin çapına bağlı Re sayısı 200 olarak alınmıştır ve silindir hareketi kütle-yay-sönüm sistemi ile modellenmiştir. Akışkan hareketi ve yapısal tepkiler iteratif olarak çözülmüştür. Bu sayede akışkan ve yapı arasındaki etkileşim uygun şekilde ele alınabilmiştir.

Silindirin tepkisi, indüklenen kuvvetler, vorteks oluşum frekansı ve iz vorteks yapısı analizleri gerçekleştirilmiştir. Bu analizlerde, yapının, $M^*=m/(\rho D^2)$ akışkan yoğunluklar oranının silindir tepkisine etkisi (burada m yapısal kütle, $\rho$ akışkanın yoğunluğu, D de silindirin çapıdır) $f_n$ /$f_s$* frekanslar oranının (burada $f_n$ yapısal frekans, $f_s$* ise rijit silindirin vorteks oluşum frekansıdır.) bir fonksiyonu olarak, indirgenmiş sönümleme parametresi Sg=0.01 sabit değeri için incelenmiştir. Sabit Strouhal sayısında, Sg, sönümleme faktörü ve M* yoğunluklar oranı çarpımı ile doğru orantılıdır.

M* kütle parametresinin 1 ile 10 arasında değişen beş ayrı değeri için inceleme yapılmıştır. Silindirin vortekslerce indüklenen tepkisinin önemli bir ölçüde olabilmesi için $f_n/f_s$* frekanslar oranının 1.0 değeri civarında daha yoğun olmak üzere 0.65 ile 2.60 arasında çeşitli değerleri için inceleme yapılmıştır. Kilitlenme " Lock on " olayını tesbit edebilmek için deplasman faz grafikleri, sürükleme, taşıma kuvvet katsayıları ve bunlara karşı gelen akış hallerinin zamanla değişimi çözülmüş ve irdelenmiştir. Sonuçlar önceki çalışmalardakilerle karşılaştırılmış ve uygunluklar bulunmuştur.

# 1. INTRODUCTION

## 1.1 Fluid – Structure Interaction Problem

A fluid-structure interaction problem of common occurrence is that of a freely vibrating bluff structure in a cross-flow. The flow-induced vibrations resulting from the shed vortices can cause structural fatigue and in certain circumstances, and lead to drastic failure of the structure. As a result, the problem has received increased attention of researchers in recent years since many modern structures use composite, lighter materials that give rise to low damping and a wide synchronization band. According to Sarpkaya [1], synchronization occurs when the natural frequency of the fluid-cylinder system is equal to the vortex shedding frequency of the vibrating cylinder. Since this cannot be determined a *priori*, synchronization can be assumed to take place whenever the natural frequency of the cylinder is approximately equal to the vortex shedding frequency of the stationary cylinder [2].

Damping models the energy dissipation during vibrations and plays an important role in the stability of the structure and its vibration amplitudes. If the dynamic behavior of the structure were to be understood properly, one would have to have knowledge of the effects of damping. Damping may arise from the structure and from the fluid surrounding the structure. Structural damping is related to the properties of the structure itself, while fluid damping is due to viscous dissipation and fluid drag, i.e. it is the result of viscous shearing of the fluid at the surface of the structure and of flow separation [3].

In our study we have carried out a rather detailed investigation of flow-induced vibrations of an elastically mounted circular cylinder in a cross-flow. A discrete vortex method incorporating a finite difference technique was used to simulate the flow field. The cylinder response was modeled by a spring-damper-mass system while the fluid motion and the structural response were solved in a way that the interactions between the fluid and the structure were handled properly.

In this study, the cylinder response, flow-induced forces, the effects of cylinder vibrations on the vortex shedding frequency and the wake vortex pattern were examined. The oncoming flow has uniform velocity and the Reynolds number based on the cylinder diameter is set at 200.

### 1.2 Early Investigations and Numerical Approaches

The flow-solid body interaction phenomenon has drawn the attention of researchers for a long time. Many researches have investigated the two-dimensional flow around bluff bodies. For example, Cheer [4,5] and Stansby & Dixon [6] have simulated both the steady and oscillatory flow around a circular cylinder using random vortex methods. Smith & Stansby [7] simulated an impulsively started flow around a circular cylinder via a Langrangian vortex solution of the vorticity equation using random walks for diffusion and the VIC (Vortex in Cell) method for convection; they obtained good agreement with experimental results. Smith & Stansby [8] also simulated the unsteady flow around a circular cylinder at post critical Reynolds numbers using a vortex method with a Baldwin & Lomax [9] turbulence model in the boundary layer. The mean pressure distribution and the vortex shedding frequency compared well with experimental data. Slaouti & Stansby [10] simulated the flow around a stationary circular cylinder in a channel for $60 \leq Re \leq 180$ and obtained Strouhal numbers which were in close agreement with those determined using finite element and spectral methods.

Blevins [11] employed a discrete vortex method to simulate the inviscid flow around an elastically supported cylinder, and predicted the vibrational response due to vortex shedding and galloping. A coordinate transformation was used to simulate the relative motion between the fluid and structure – this implies a quasi-steady assumption. The predicted maximum vibrational response agreed well with experimental results but the lock-in region between vortex shedding and structural frequencies was narrower than suggested by experimental results. Furthermore, the vibrational response did not show the sharp increase in amplitude near lock-in. The reason for this discrepancy is probably due to the fact that no attempt was made to consider the flow viscosity, i.e., the vortices were not subject to diffusion.

A discrete vortex method and operator-splitting technique was employed by Meneghini & Bearman [12] to simulate the flow around a circular cylinder oscillating normal to the flow, but in their method the diffusion equation was solved using a finite difference scheme using the same mesh as that employed to solve the Poisson's equation for stream function [13].

### 1.3 Advantages of Using Vortex Methods for Fluid-Structure Interaction Problem

Flow-induced vibration problems are often experienced in various engineering fields. In order to understand and analyze their causes and mechanisms, the numerical simulation method is considered to be one of the efficient tools, because the numerical method is able to avoid some difficulties usually found in experiments, such as boundary condition effects, uncertainty of measurement and control of flow or experimental conditions. On the other hand, the numerical analysis of a high Reynolds number flow around moving or oscillating boundary and body with the aid of the finite difference (FDM), finite volume (FVM) or finite element method (FEM) has also some difficulties related with the treatment of fine grids around the boundary surface and the validity of turbulence model. For the engineering purposes, development of an accurate, simple and robust numerical method has been required [14].

The vortex methods, which have been developed for thirty years and applied to analysis of complex vortical flows and unsteady viscous flows at high Reynolds numbers, seem to be suitable for the analysis of flow induced vibration problems, because they are grid free calculation methods, and so they are able to overcome the difficulty of treatment of moving boundary conditions in FDM, FVM and FEM. Recently, Kamemoto applied their vortex method to a sort of simulation on the flow induced vibration problems such as a freely oscillating gate, a forced oscillating circular or rectangular cylinder in a uniform flow [15] and an analysis of unsteady flow through a centrifugal-pump impeller with moving boundary condition. The history, mathematical basis and application of the vortex method are well reviewed by Kamemoto [16].

## 2. MATHEMATICAL MODEL

In this study, a 2D circular cylinder undergoing vibration in both in-line and cross-flow directions is simulated and the cylinder response is calculated. A discrete vortex method based on the Vortex-in-Cell formulation incorporating viscous diffusion is used for the simulation. Following the establishment of the solution technique, necessary reference system transformation is made and the spring-mass-damper system defining the vibrating cylinder is presented.

For solution of a flow-induced vibration of a 2D circular cylinder, the governing equations are presented below.

### 2.1 Governing Equations

The fundamental equation of a flow for a Newtonian fluid is the equation derived from the balance of momentum namely the Navier-Stokes equation. The balance of momentum for a fluid can be written as [17];

$$\rho \frac{D\vec{U}}{DT} = \rho \vec{g} + \nabla \vec{\sigma} \tag{2.1}$$

By taking $\vec{\sigma}$ in consideration according to Stoke's postulates, for an incompressible and constant-viscosity fluid, this equation becomes:

$$\rho \frac{D\vec{U}}{Dt} = \rho \vec{g} - \nabla p + \mu \nabla^2 \vec{U} \tag{2.2}$$

The gravity term is negligible in most cases so the two dimensional form of the Navier-Stokes equation becomes,

$$\frac{\partial u}{\partial t} + u\frac{\partial u}{\partial x} + v\frac{\partial u}{\partial y} = -\frac{1}{\rho}\frac{\partial p}{\partial x} + \nu\left[\frac{\partial^2 u}{\partial x^2} + \frac{\partial^2 u}{\partial y^2}\right] \tag{2.3}$$

$$\frac{\partial v}{\partial t} + u\frac{\partial v}{\partial x} + v\frac{\partial v}{\partial y} = -\frac{1}{\rho}\frac{\partial p}{\partial y} + \nu\left[\frac{\partial^2 v}{\partial x^2} + \frac{\partial^2 v}{\partial y^2}\right] \tag{2.4}$$

Taking the curl of these two equations and thus eliminating the pressure from them gives “Vorticity Transport Equation” in two dimensions, that is

$$\frac{D\omega}{Dt} = \nu\nabla^2\omega \tag{2.5}$$

$$\frac{\partial\omega}{\partial t} + \left(\vec{U}\nabla\right)\omega = \nu\nabla^2\omega \tag{2.6}$$

where “ ω ” is defined here as “fluid vorticity”.

$$\omega = \frac{\partial v}{\partial x} - \frac{\partial u}{\partial y} \tag{2.7}$$

Consequently, from the incompressibility assumption $div\vec{U} = 0$,

$$\frac{\partial u}{\partial x} + \frac{\partial v}{\partial y} = 0 \tag{2.8}$$

and definition of the stream funtion ψ as;

$$\frac{\partial\psi}{\partial y} = u \qquad \frac{\partial\psi}{\partial x} = -v \tag{2.9}$$

gives the Poisson’s equation;

$$\nabla^2\psi = -\omega \tag{2.10}$$

## 2.2 Splitting the Vorticity Trasport Equation

The method employed originates from the work of Chorin [18], who considered the two-dimensional Navier-Stokes equations written in the form of vorticity

$$\frac{\partial\omega}{\partial t} + \left(\mathbf{u}\vec{U}.\nabla\right)\omega = \nu\nabla^2\omega \tag{2.11}$$

where the terms $\left(\mathbf{u}\vec{U}.\nabla\right)\omega$ and $\nu\nabla^2\omega$ represent the rate of change of vorticity due to convection and molecular diffusion, respectively. Because the flow being considered is two-dimensional the vorticity, ω, is a scalar term.

Chorin [18] suggested splitting the Navier-Stokes equations into linear diffusion and nonlinear convective parts as shown below

$$\frac{\partial \omega}{\partial t} = -\left(\overrightarrow{U}.\nabla\right)\omega \tag{2.12}$$

and

$$\frac{\partial \omega}{\partial t} = \nu\nabla^2\omega \tag{2.13}$$

These equations are then solved using a fractional time step method, where the equations are solved sequentially rather than simultaneously. In this sequential solution, at each time step the diffusion equation is solved using the state of the flow at the end of the previous time-step as the new initial condition. The convection equation is then solved using as initial conditions the solution of the diffusion equation. The vorticity in the flow is represented by a large number of discrete point vortices, which at each time-step in the simulation are created on the cylinder surface to satisfy the no-slip boundary condition. These vortices are then convected downstream as dictated by diffusion and convection.[13]

### 2.3 Solution of Poisson Equation

The stream function values required to determine the convection velocities of the discrete vortices are obtained using the Poisson's equation in its circulation form:

$$\nabla^2\psi = -\frac{\Gamma}{A} \tag{2.14}$$

The Poisson's equation is solved using the Fast Fourier Transform (FFT) technique. If the solution domain is rectangular NxM grid, N, being the number of mesh points in x direction in which the Fourier transformation is taken, is restricted to be power of 2, i.e. $N=2^k$ (k=1,2,…) [19].

Taking the Fourier transform along x direction reduces Poisson's equation into a tridiagonal system of equations. The boundary conditions at top and bottom in transformation plane are given as Dirichlet type. For surface, the stream function value is zero. Since the Poisson's equation is linear the superposition principle is applied and the stream function corresponding to a non-zero circulation distribution is added onto the stream function of the basic flow.

The discretized form of Poisson's equation is given in Appendix A1

## 2.4 Conformal Transformation

In order to study the flow around a circular cylinder a conformal transformation is used. The analytical expression of this transformation from the semi-finite computational plane ($\zeta$) to the physical cylinder plane (z) is

$$z=R\exp(-i\alpha\zeta) \tag{2.15}$$

with

$$z=x+iy \quad \zeta=\xi+i\eta \tag{2.16}$$

where R is the radius of the circular cylinder, $\alpha$ is step size in angular direction and $\eta=0$ represents the cylinder wall in the transformed plane. The mesh size in the $\xi$ -direction is uniform while a stretched mesh is used in the $\eta$ -direction in order to resolve accurately the boundary layer on the cylinder (Figure 2.1), keeping the outer boundary of the mesh as far from the cylinder center as possible at the same time [2].

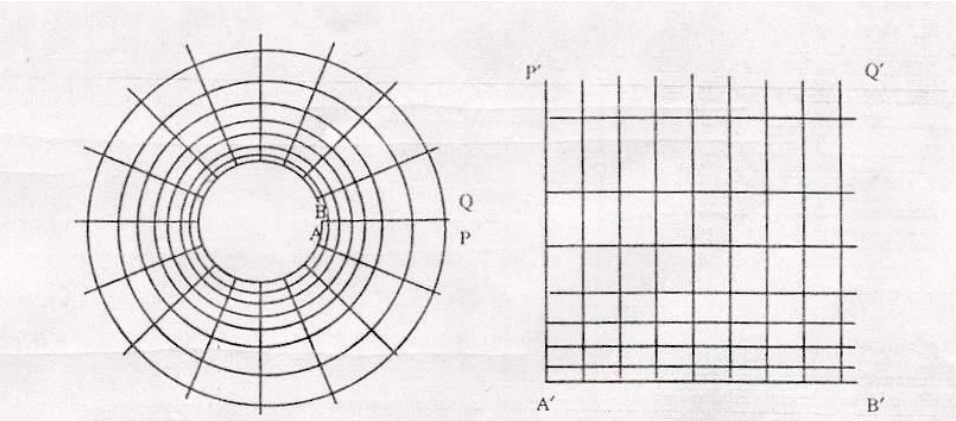


**Figure 2.1 The meshes in both physical and computational planes**

The Jacobian of the transformation is given as

$$J=\left|\frac{dz}{d\varsigma}\right|^2=\left[\alpha\,\mathrm{Re}\,xp(\alpha\eta)\right]^2 \tag{2.17}$$

In this study, a mesh with 170 points in the radial direction and 128 points in the angular direction has been used (Figure 2.1). The radius of the circular cylinder R is

taken as 1.0 and $\alpha$ step size in angular direction is 0.05. A stretched grid is used in the radial direction in order to resolve accurately the cylinder boundary layer. Corresponding to the stretched grid in the physical plane, expression of the stretched grid in $\eta$ -direction is given as follows:

$$Y(j) = YGB * [\exp((j-1) * YGA) - 1] \quad (2.18)$$

$$YGA = (MY - 1 - BGA) / (YGA_0) \quad (2.19)$$

$$YGB = BGA * YGB_0 \quad (2.20)$$

$$BGA = GFR * MY \quad (2.21)$$

In this study, MY=170, GFR=0.77, $YGA_0$=2.4, $YGB_0$=0.0275 are taken and the increments in $\eta$ -direction ($Y_{INC}$) are obtained by changing J from 1 to MY,

$$Y_{INC} = Y(J) - Y(J-1) \quad (2.22)$$

First increment is 0.067.

### 2.5 The Vortex-in-Cell Method

As the flow evolves, the number of discrete vortices emited into the flow field increases and eventually makes the use of fully Langrangian method of approximation with direct summation (i.e. Bio-Savart induction principle) almost impracticable. To overcome this difficulty a mixed Eulerian-Langrangian scheme is employed. The Vortex-in-Cell (VIC) method is preferred for calculation of the velocity field through the use of Poisson's equation. The main advantage of the VIC method is that it requires in the order of $M.Log_2M$ operations when performed on a grid of M points, while the number of operations with the Bio-Savart calculation method reaches order of $N^2$ operations for a flow field of N vortices. The VIC method provides also the desingularization of the velocity field by smearing the vorticity over a cell area [19].

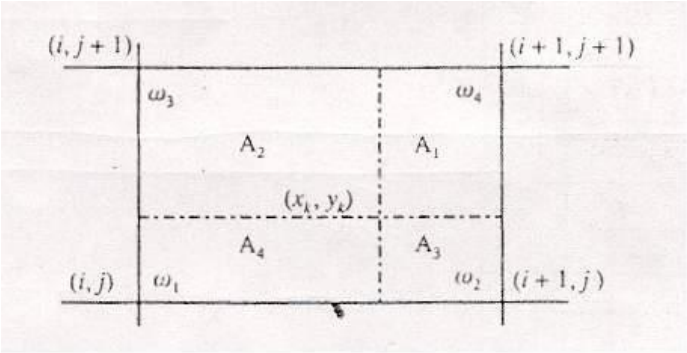


**Figure 2.2 The area-weighting distribution scheme**

For the purpose of solving Poisson's equation, the circulations of each vortex need to be distributed to the four surrounding mesh points. Herein, a bilinear area-weighting scheme is used. On a Cartesian mesh (Figure 2.2) this interpolation, for a vortex of circulation Γ, is calculated by

$$\Gamma_{(m)} = \frac{\Gamma . A_{(m)}}{A} \tag{2.23}$$

where A is the total area of the mesh cell (Figure 2.2). The total circulation of a mesh point is defined by summing the contribution from all the vortices in the four surrounding cells.

The stream function values are obtained at every mesh point (i,j) from the solution of the Poisson's equation. Then the mesh velocities are calculated using

$$u_{(i,j)} = \frac{1}{J}\frac{\partial \psi_{(i,j)}}{\partial \eta} \tag{2.24}$$

$$v_{(i,j)} = -\frac{1}{J}\frac{\partial \psi_{(i,j)}}{\partial \xi} \tag{2.25}$$

and the velocity components of each discrete vortex are determined from an area weighting scheme in reversed direction (Figure 2.2)

$$u_k = \sum_{m=1}^{4} u_{(m)} \frac{A_{(m)}}{A} \quad \text{and} \quad v_k = \sum_{m=1}^{4} v_{(m)} \frac{A_{(m)}}{A} \tag{2.26}$$

## 2.6 Diffusion of Vorticity and Boundary conditions on Circulation

Under conformal transformation, the diffusion part of the Vorticity Transport equation (2.11), which is given in equation (2.13), takes the form of

$$\frac{\partial(\Gamma / A)}{\partial t} = \nu \left[ \frac{\partial^2(\Gamma / A)}{\partial \xi^2} + \frac{\partial^2(\Gamma / A)}{\partial \eta^2} \right] \frac{1}{J} \tag{2.27}$$

The finite difference technique is applied to this equation with proper discretization allowing explicit calculations in x direction and implicit in y direction. The finite difference forms of this equation were given in Appendix A2

The diffusion equation is solved subject to the no-slip boundary condition at the surface. The first order approximation for the surface vorticity, in its circulation form [20] is employed.

$$\Gamma_w = -\frac{2(\psi_{w+1} - \psi_w)}{h} \Delta x \tag{2.28}$$

where subscript “w” stands for the value at the wall, “w+1”, for the neighboring grid to the wall; “h” is the distance of neighboring grid to the wall and Δx is the constant mesh spacing in x direction. Since the flow is impulsively started, the wall circulation values at the start of the motion are determined by the stream function values of the basic flow.

For the solution of the Poisson’s Equation for the stream function periodicity is imposed at the right and left boundaries of the computation plane, and at the upper boundary the stream function values induced by the discrete vortices and their images in the body are taken as the boundary condition. At the lower boundary describing the wall, the stream function value is taken as zero. After calculating the diffused vorticity across the mesh and therefore determining the new vorticity field, the Poisson’s Equation is solved again and the stream function values at grid points are used to calculate the convection velocities of vortices. Consequently, the vortices are convected to their new positions at the end of each time step.

## 2.7 Convection of Vorticity

Solution of the convection equation involves determining the velocity on each vortex induced by the other vortices in the flow. In principle, this can be done using the Biot-Savart law; however, the number of calculations required at each time-step is of order $N^2$, where N is the number vortices in the flow which typically becomes very large. To overcome this problem the vortex-in-cell, VIC, method previously developed by Christiansen [21] was used, where an orthogonal mesh represents the flow field and vorticity in each cell of the mesh is allocated to the four surrounding mesh points using an area-weighting scheme.

$$\Gamma_{(m)} = \frac{\Gamma . A_{(m)}}{A} \tag{2.29}$$

$$(u,v) = \frac{(u,v)A_{(m)}}{A} \tag{2.30}$$

Poisson Equation is then solved for the stream function of the flow and eventually the velocities induced by the vortices in the flow field are determined from:

$$u = \frac{\partial \psi}{\partial y}\left|\frac{d\xi}{dz}\right|^2 \tag{2.31}$$

$$v = -\frac{\partial \psi}{\partial x}\left|\frac{d\xi}{dz}\right|^2 \tag{2.32}$$

Now, knowing the mesh velocities, an area weighting scheme, in reversed direction (2.30) then gives the convection velocities of the discrete vortices as follows;

$$u_p = \sum_{m=1}^{4} \frac{u_{(m)} A_m}{A} \tag{2.33}$$

$$v_p = \sum_{m=1}^{4} \frac{v_{(m)} A_m}{A} \tag{2.34}$$

Consequently, the vortices are advanced to their new location as;

$$\xi_p(t+\Delta t) = \xi_p(t) + u_p(t)\cdot \Delta t \tag{2.35}$$

$$\eta_p(t+\Delta t) = \eta_p(t) + v_p(t)\cdot \Delta t \tag{2.36}$$

## 2.8 Force Calculation

The force acting on the rigid boundary is due to the pressure and skin friction distributions. Since pressure is eliminated from the governing equations when they are written in terms of vorticity, it is not given as a direct result of the flow field calculation. Both pressure and skin friction distributions are calculated with known vorticity distribution around the cylinder surface. Force coefficients are then calculated by suitably integrating the pressure and skin friction contributions.

If the Navier-Stokes equations in primitive variables are considered at the wall together with the definition of vorticity and the no-slip boundary condition, it leads to the following expression.

$$\frac{1}{\rho}\cdot\left.\frac{\partial p}{\partial s}\right|_{wall} = -\nu\left.\frac{\partial \omega}{\partial n}\right|_{wall} \tag{2.37}$$

where p is the pressure, ρ the density of the fluid and n and s are the coordinates in the normal and tangential directions, respectively. The pressure distribution around the surface of the cylinder is obtained by integrating this expression in the form

$$\Delta p_{(i,0)} = -\nu\cdot\Delta\omega_{(i,0)}\cdot\frac{\Delta s}{\Delta n} \tag{2.38}$$

where $\Delta p_{(i,0)}=p_{(i+1/2)}-p_{(i-1/2)}$, $\Delta\omega_{(i,0)}=\omega_{(i,1)}-\omega_{(i,0)}$ and Δn and Δs are the increments in the n and s directions, respectively.

The skin friction contribution is obtained from the definition of shear stress at the wall and the definition of vorticity, which yields

$$\tau_{(i,0)} = -\mu\cdot\omega_{(i,0)} \tag{2.39}$$

where $\tau_{(i,0)}$ is the skin friction at the wall, and μ is the dynamic viscosity. After considering the contributions from skin friction and pressure, the force components are resolved in the two directions x,y in the physical plane, yielding $F_x$ and $F_y$. These forces are then non-dimensionalized as follows,

$$C_L = \frac{2F_y}{\rho U^2 D} \tag{2.40}$$

$$C_D = \frac{2F_x}{\rho U^2 D} \tag{2.41}$$

$C_L$ and $C_D$ are known to be the lift and drag coefficients respectively.

### 2.9 Spring-Mass-Damper System

The response of an elastically mounted and linearly damped cylinder satisfies the following equation of motion in y direction [17]

$$m\ddot{Y} + c\dot{Y} + kY = F_y \tag{2.42}$$

and in x direction

$$m\ddot{X} + c\dot{X} + kX = F_x \tag{2.43}$$

where $F_y$ and $F_x$ are the hydrodynamic forces in y direction and in x direction, respectively. When inertia effects are taken into account the equations (2.42) and (2.43) becomes

$$m\ddot{Y} + c\dot{Y} + kY = F_{cy} + \rho V\ddot{Y} \tag{2.44}$$

$$m\ddot{X} + c\dot{X} + kX = F_{cx} + \rho V\ddot{X} \tag{2.45}$$

where $F_{cy}$ and $F_{cx}$ are instantaneous values of the computed hydrodynamic force.

If we arrange the equations (2.44) and (2.45) becomes

$$\left(1-\frac{\rho}{\rho_s}\right)\ddot{Y} + 2\xi_s\left(\pi\frac{f_n D}{U}\right)\dot{Y} + \left(\pi\frac{f_n D}{U}\right)^2 Y = \frac{\rho}{\rho_s}\frac{C_L}{\pi} \tag{2.46}$$

$$\left(1-\frac{\rho}{\rho_s}\right)\ddot{X} + 2\xi_s\left(\pi\frac{f_n D}{U}\right)\dot{X} + \left(\pi\frac{f_n D}{U}\right)^2 X = \frac{\rho}{\rho_s}\frac{C_D}{\pi} \tag{2.47}$$

The derivatives of this equation were given in Appendix A3

The main parameters used in this study will be the density ratio of the fluid to the cylinder ($\rho/\rho_s$), the damping parameter ($\xi_s$) and non-dimensionalized natural structural frequency of the cylinder ($f_n$.D/U). With these parameters we will compare the results easily.

## 2.10 Numerical Algorithm

Briefly, a typical application of the algorithm is as follows.

1. Make transformation between a circle and a rectangle by use of equation (2.15)
2. Advance time by $\Delta t$
3. Interpolate circulation onto mesh
4. Solve Poisson's Equation for $\psi$ around body
5. Create circulation at solid boundary and diffuse circulation for entire mesh
6. Solve Poisson's equation for entire mesh
7. Create modified circulation at solid boundary
8. Diffuse circulation adjacent to solid boundary
9. Release or join diffused circulation
10. Evaluate force and pressure distributions
11. Difference stream function to obtain velocity field
12. Interpolate velocity onto point vortices and convect them
13. Repeat steps 2 through 12 for the next time step

## 3. RESULTS AND CONCLUSION

The incompressible, viscous two-dimensional cross-flow over an elastically mounted circular cylinder has been simulated using a discrete vortex approach. Simulations and characteristics of flow have been performed at Re=200 for which the flow is still laminar.

A mesh with 170 points in the radial direction and 128 points in the angular direction has been used. A stretched grid is used in the radial direction in order to resolve accurately the cylinder boundary layer (Figure 2.1) while keeping the outer extent of the mesh as large as possible.

For the in-line and cross-flow oscillations of the cylinder immersed into a uniform flow, the cylinder is allowed to oscillate only after Time=10.25, at which an initial period of vortex shedding is completed. The equation of motion the oscillating cylinder is solved by a fourth order Runge-Kutta method.

### 3.1 Rigid Circular Cylinder at Re=200

In order to establish a baseline for comparison a uniform flow past a rigid circular cylinder at Re=200 is calculated first. Figure 3.1 shows the time histories of the lift and drag coefficients. It can be seen that the lift force settles to a regular sinusoidal function with a value of Clrms=0.72 (Figure 3.1). Similarly, the drag force also settles to a periodic behaviour with a mean value 1.43 as compared to 0.8 and 1.32 obtained previously by Zhou [2].

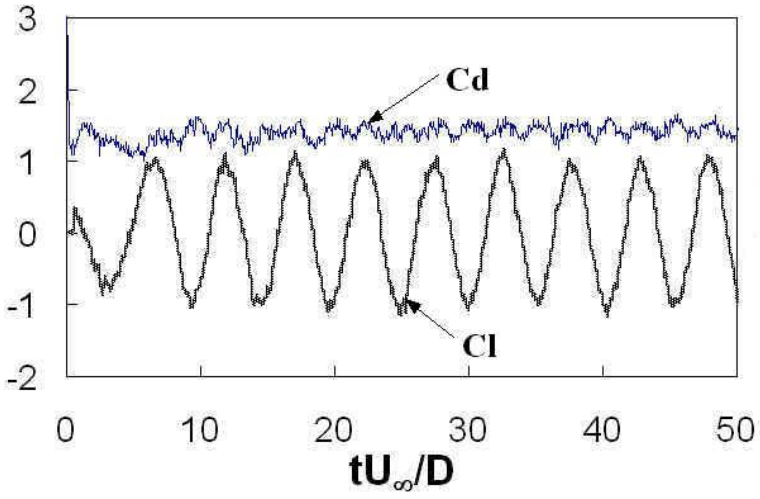


**Figure 3.1 Force time histories for a rigid cylinder Re=200**

The vortex pattern in the wake shown in Figure 3.2 composes of negative and positive staggered vortices, the well known Karman vortex street. A good agreement is obtained in comparison with other numerical and experimental studies [2]

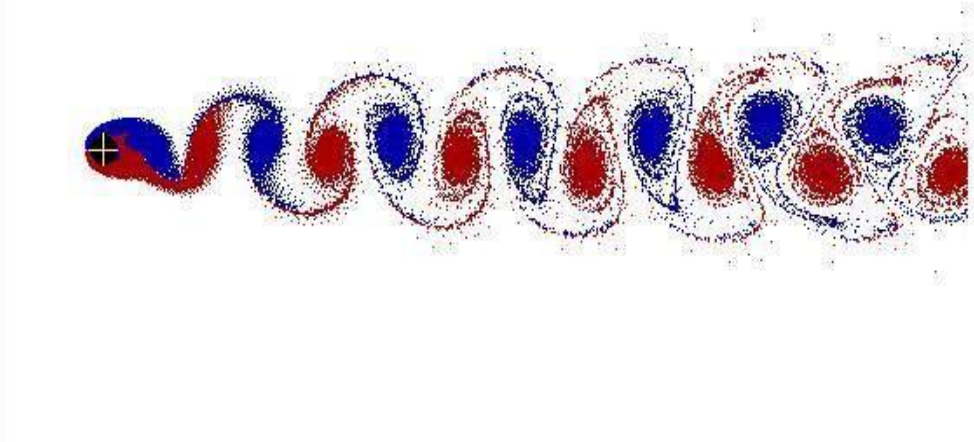

**Figure 3.2 The vortex pattern in the wake of a rigid cylinder Re=200 for dimensionless time( $U_\infty/D$ ) = 50**

Figure 3.3 show that the St*=0.1931 for the lift oscillations and the dimensionless frequency of the drag force is determined to be 0.4069. Note that in a previous study Zhou [2] St*= 0.1922 for $C_L$ and 0.3853 for $C_D$.

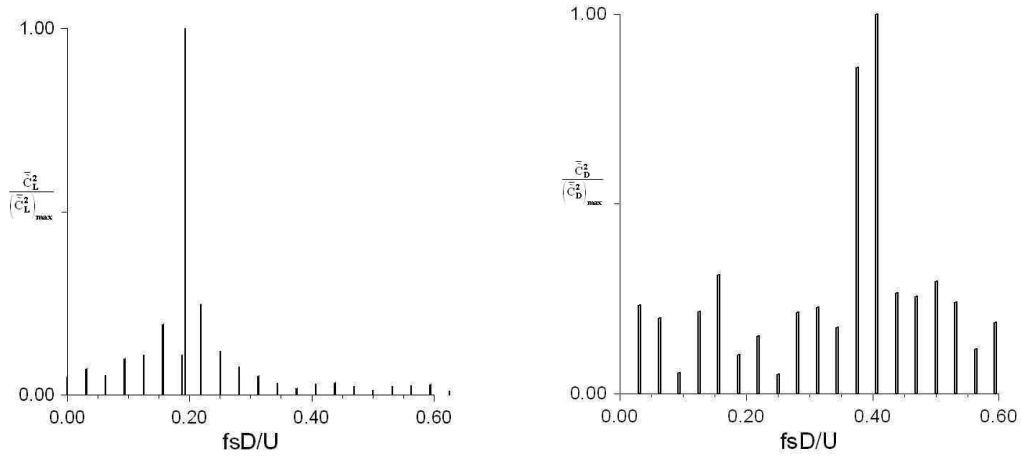


**Figure 3.3 Power Spectrum of $C_L$ and $C_D$ fluctuations, Re=200**

### 3.2 Choices of Structural Parameters

The computation time step ($\Delta t\ U_\infty / D$) is set to 0.0025 for all cases. Calculations were then carried out for an elastically mounted circular cylinder with two degrees of translational freedom for a number of cases at Re=200. For comparison with Zhou's [2] study, we must define a parameter; reduced damping parameter Sg which is,

$$Sg = 8\pi^2 St^{*2} \alpha M^* \tag{3.1}$$

Here $St^* = f_s^* D / U_\infty$ is the Strouhal number, $M^* = m / \rho D^2$ is the mass ratio, $\alpha$ is the damping factor in the structural dynamic equations which is equal to $\xi_s$ in our study. D is the cylinder diameter, $U_\infty$ is the undisturbed freestream velocity, $f_s^*$ is the vortex shedding frequency of the rigid cylinder, m is the mass per unit length of the cylinder and $\rho$ is the fluid density.

In our study, we set the reduced damping parameter Sg=0.01 and calculated the $\xi_s$ value corresponding to a chosen M* value. In order to have a significant vortex-

induced response, the frequency-ratio, $f_n/f_s^*$, ranges from 0.65 to 2.6 with most of the cases concentrated around $f_n/f_s^*=1$.

The main parameters used in this study will be the density ratio of the fluid to the cylinder ($\rho/\rho_s$), the damping parameter ($\xi_s$) and non-dimensionalized natural structural frequency of the cylinder ($f_n.D/U$) which is inverse of the reduced velocity Vr. Corresponding to St*=0.1931 in the rigid case the $f_n/f_s^*$ ratio is calculated as follows,

$$\frac{1}{Vr} = f_n \, D \diagup U_\infty \tag{3.2}$$

$$St^* = f_s^* D / U_\infty \tag{3.3}$$

so

$$\frac{f_n}{f_s^*} = \frac{1}{0.1931 * Vr} \tag{3.4}$$

For each value of M* considered the reduced velocity Vr of the corresponding $f_n/f_s^*$ is changed within the interval shown in Table 3.1.

**Table 3.1** Structural parameters of the cases with Sg=0.01

| **Case** | **M*** | **$\rho/\rho_s$** | **$\xi_s$** | **Vr** | **$f_n/f_s^*$** |
|---|---|---|---|---|---|
| **1** | 1 | 0.7854 | 0.003400 | 2.0 - 8.0 | 2.60 - 0.65 |
| **2** | 1.5 | 0.5236 | 0.002270 | 2.0 - 8.0 | 2.60 - 0.65 |
| **3** | 2 | 0.3927 | 0.001700 | 2.0 - 8.0 | 2.60 - 0.65 |
| **4** | 3 | 0.2618 | 0.001133 | 2.0 - 8.0 | 2.60 - 0.65 |
| **5** | 10 | 0.07854 | 0.000340 | 2.0 - 8.0 | 2.60 - 0.65 |

Each calculation for a given set of structural parameters requires about 7 hour of computer time on a PC with P III-600 co-processor to reach a non-dimensional time based on the diameter D of 50.

### 3.3 Streamwise and Transversely Oscillating Cylinder in a Stream

#### 3.3.1 CASE – 1

The time histories of lift and drag coefficients, transverse and streamwise displacements and displacement phase plots (Lisaju figures) are shown in Figure B1.5.

The mean drag coefficient $C_{Dmean}$, the root mean square values of the cross-flow amplitude Yrms of the cylinder, the lift coefficient Clrms, mean streamwise-flow amplitude Xmean, and the vortex shedding frequency ratio $f_s/f_s*$, versus the $f_n/f_s*$ are shown in Figure 3.4 .

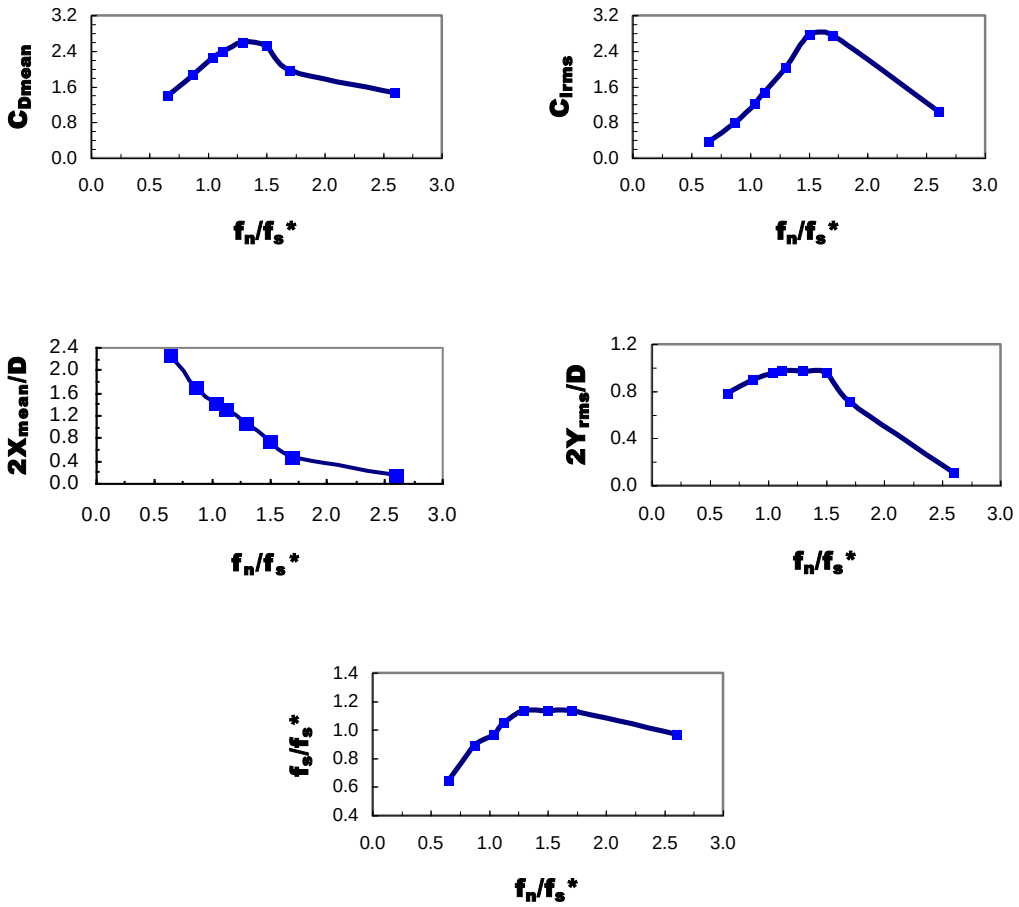


**Figure 3.4 Results for the Case-1 at Re=200 and Sg=0.01**

It is seen that all parameters except the $2X_{mean}/D$ behave similarly. That is, as the ratio fn/fs* increases, the parameters first increase, they reach their maxima, then decrease and approach a value representative of that of the rigid circular cylinder (Figure 3.4). It is noted that both the transverse oscillation amplitude of the cylinder and the drag coefficient reach their maximum values at the frequency ratios fn/fs*=1.30 where the maximum values for $C_{Dmean}$ and $2Y_{rms}/D$ are 2.59 and 0.97 respectively.

For the $f_n/f_s^*=2.60$ the response is small and the forces $C_L$ and $C_D$ are similar to those for the rigid circular cylinder (Figure 3.1). Cylinder is almost stationary. We can extract the same result from the displacement phase plot (Figure B1.5). The figure 8 means Y displacement's frequency is two times of the x displacement's frequency. In addition to that, the vibration is not violent. As the $f_n/f_s^*$ decreases, such as $f_n/f_s^*=1.70$, the motion of cylinder seems to be disorganized, the cylinder oscillation amplitude is modulated or "beating". This will easily seen by the history of forces and displacement plots. For $f_n/f_s^*=1.30$ the locking on is achieved. We can see from the power spectrum of the lift oscillations and drag oscillations (Figure B1.3, B1.4) that the vortex shedding frequency have a larger value at $f_n/f_s^*=1.30$ in comparison with those at the other frequency ratios. On each side of the locking on region, forces acting on the cylinder are smaller as compared to the values at the locking-on region. In Figure 3.5 we see the comparison of the vortex pattern in the wake of the elastically mounted circular cylinder at different frequency ratios. Each vortex pattern corresponds to an instant at which lift coefficient is minimum.

Comparison of the y oscillation amplitude with that obtained by Zhou is given in Figure 3.6.

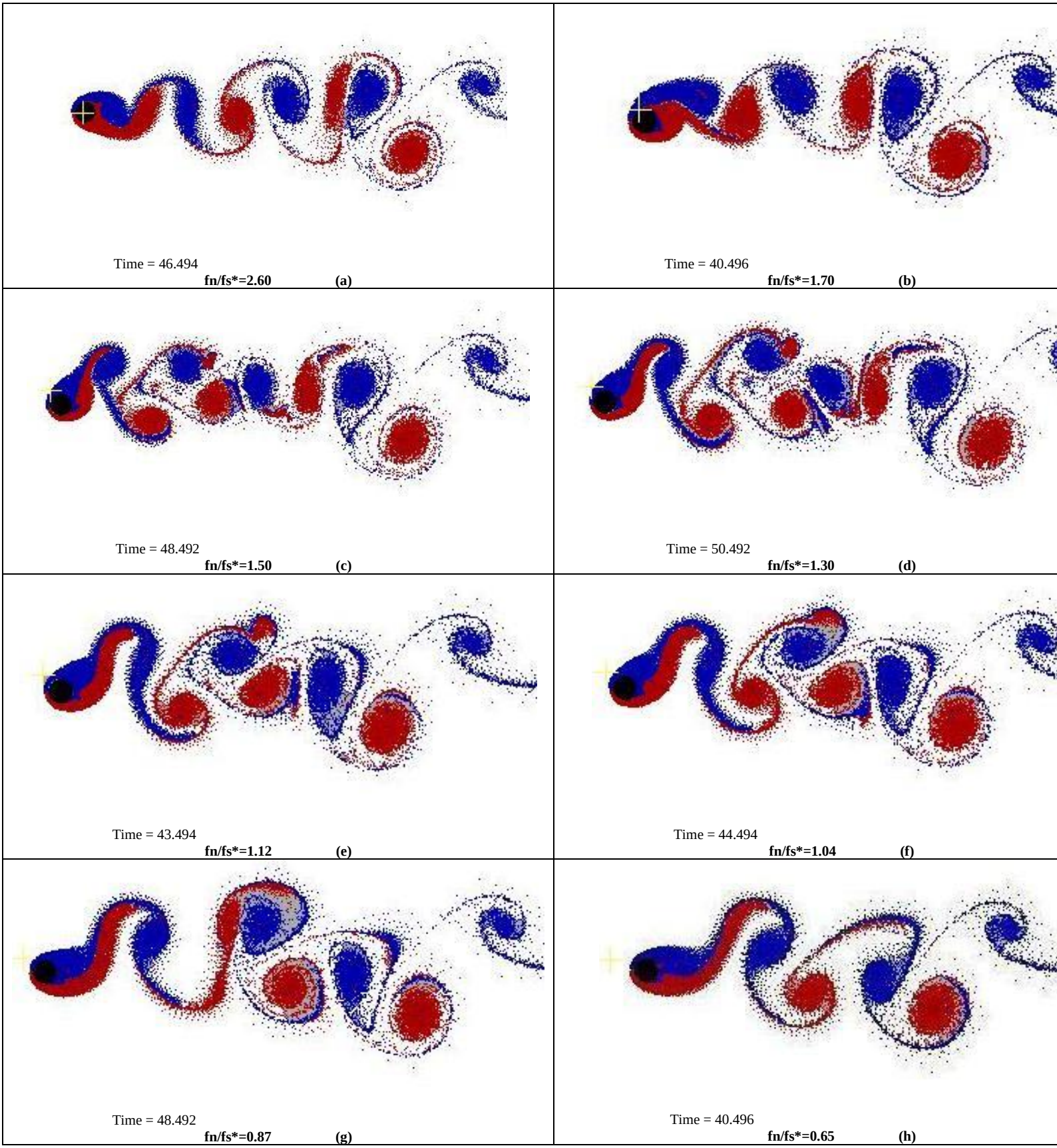


**Figure 3.5 Variation of wake structure as function of $f_n/f_s^*$ ratio for Case-1**

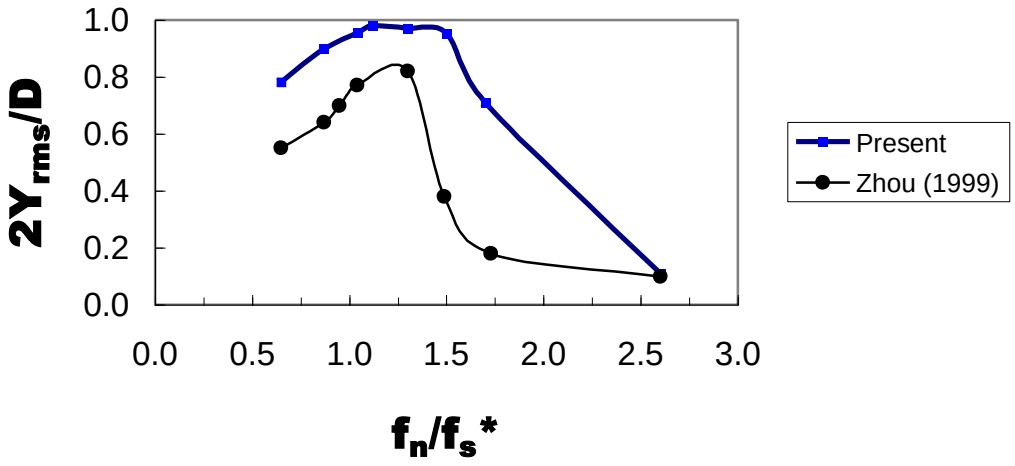


**Figure 3.6 Variation of the root mean square oscillation amplitude $2Y_{rms}/D$ as a function of $f_n/f_s^*$ for the Case-1**

### 3.3.2 CASE – 2

The time histories of computed values of $C_L$, $C_D$, Y/D and X/D for various frequency ratios are given in Appendix B2. In this case the mass ratio and the damping factor are less than those for the case-1. We see from displacement phase plot (Figure B2.5) that the locking-on region is between the frequency ratios $f_n/f_s^*$=1.30 and fn/fs*=1.04.

It is noted that both the transverse oscillation amplitude of the cylinder and the drag coefficient reach their maximum values at the frequency ratios $f_n/f_s^*$=1.30 where the maximum values for $C_{Dmean}$ and $2Y_{rms}/D$ are 2.55 and 0.92 respectively (Figure 3.8).

When the mass ratio is increased, maximum values of the drag and lift coefficient values decrease. After the locking on region, the force acting on the cylinder decrease and eventually reaches to values similar to those for the rigid cylinder case (Figure B2.1, B2.2). The wake structure of this case is given in Figure 3.7. Within the locking-on region the vortex street shows a double shear layer formation.

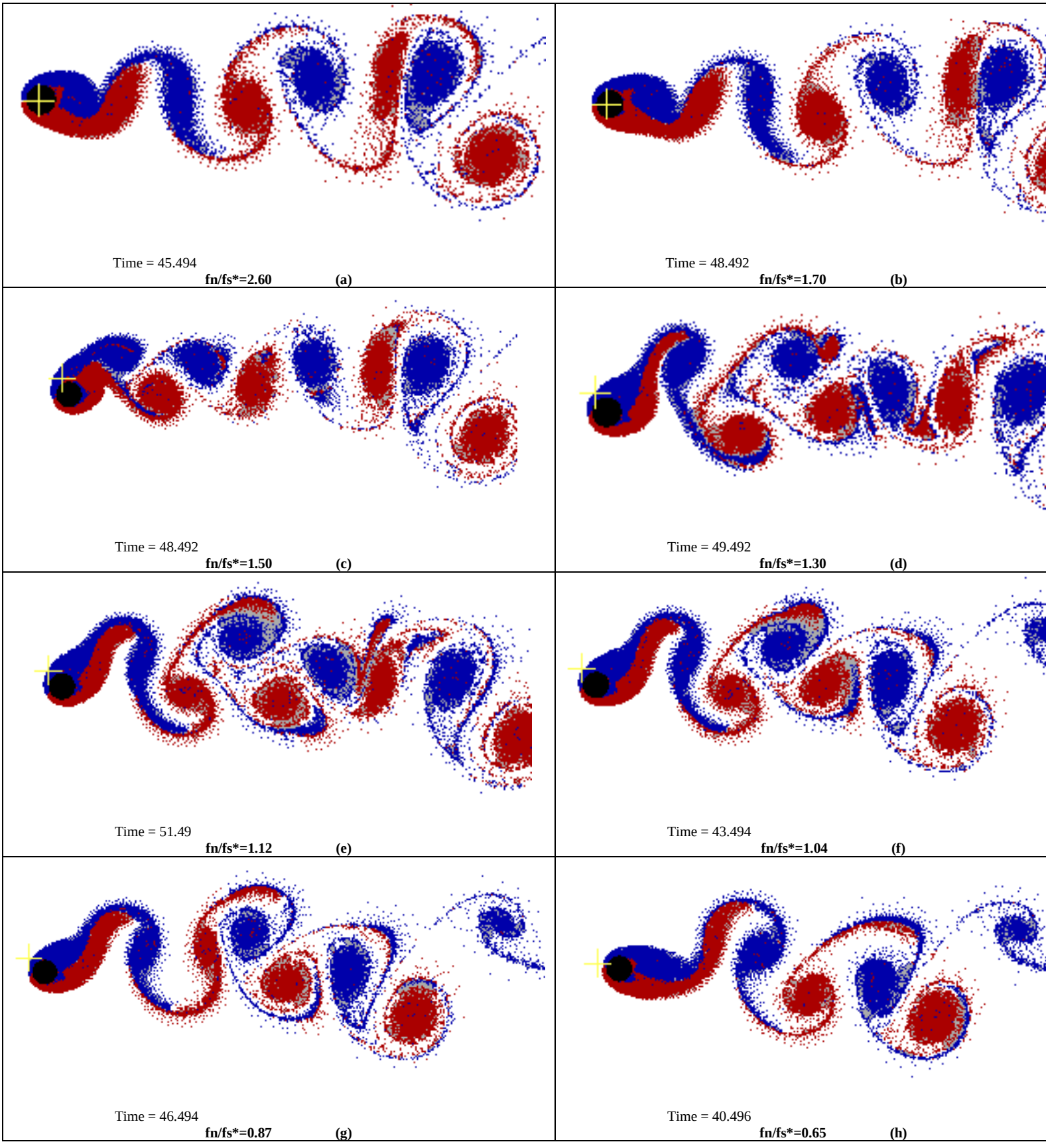


**Figure 3.7 Variation of wake structure as function of $f_n/f_s^*$ ratio for Case-2**

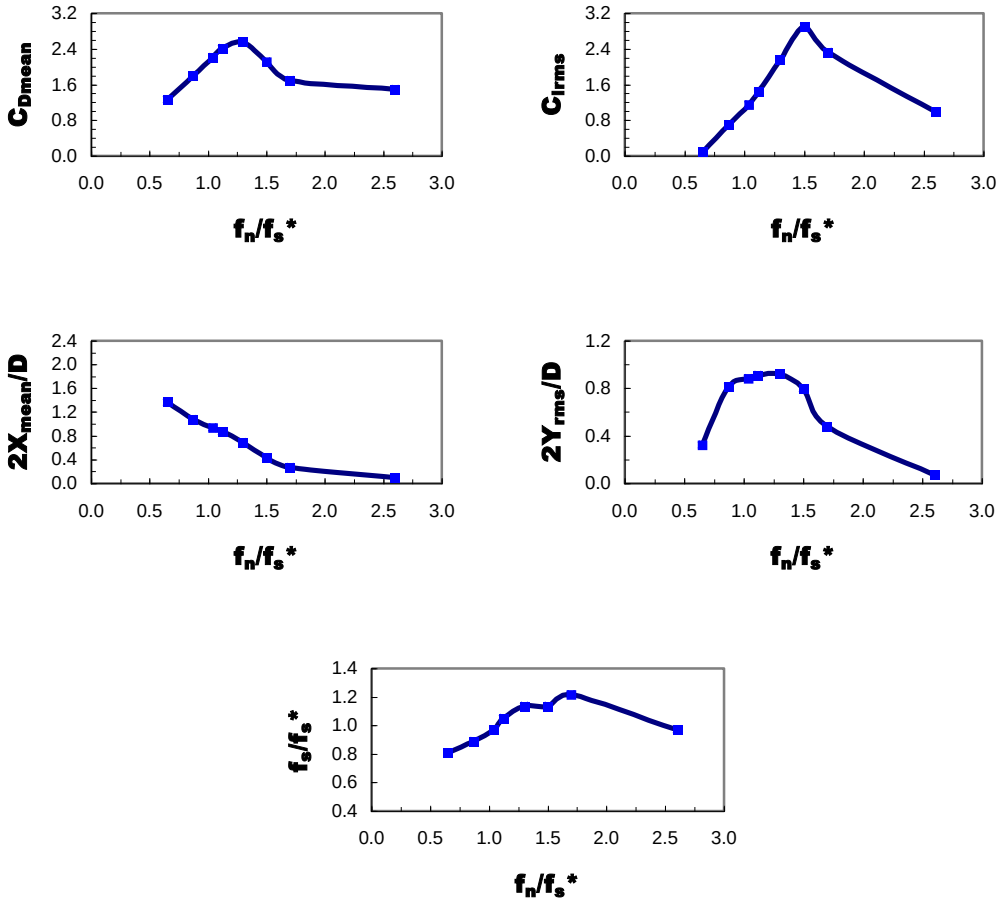


**Figure 3.8 Results for the Case-2 at Re=200 and Sg=0.01**

### 3.3.3 CASE – 3

In this case the locking-on is obtained somewhere near $f_n/f_s^*=1.30$ (Figure 3.10). In the displacement phase plot (Figure B3.5), an 8 like shape is obtained when $f_n/f_s^*=1.30$. After this regime when $f_n/f_s^*=0.87$ and $f_n/f_s^*=0.65$ the responses are small and the forces $C_L$ and $C_D$ are similar to those for the rigid circular cylinder (Figure B3.1, B3.2 and Figure 3.9g, h).

The maximum transverse oscillation amplitude of the cylinder and the drag coefficient are 2.54 and 0.90 respectively. For the $f_n/f_s^*=1.70$ and $f_n/f_s^*=1.50$ we see again the beating patterns (Figure B3.1, B3.2, B3.3, B3.4).

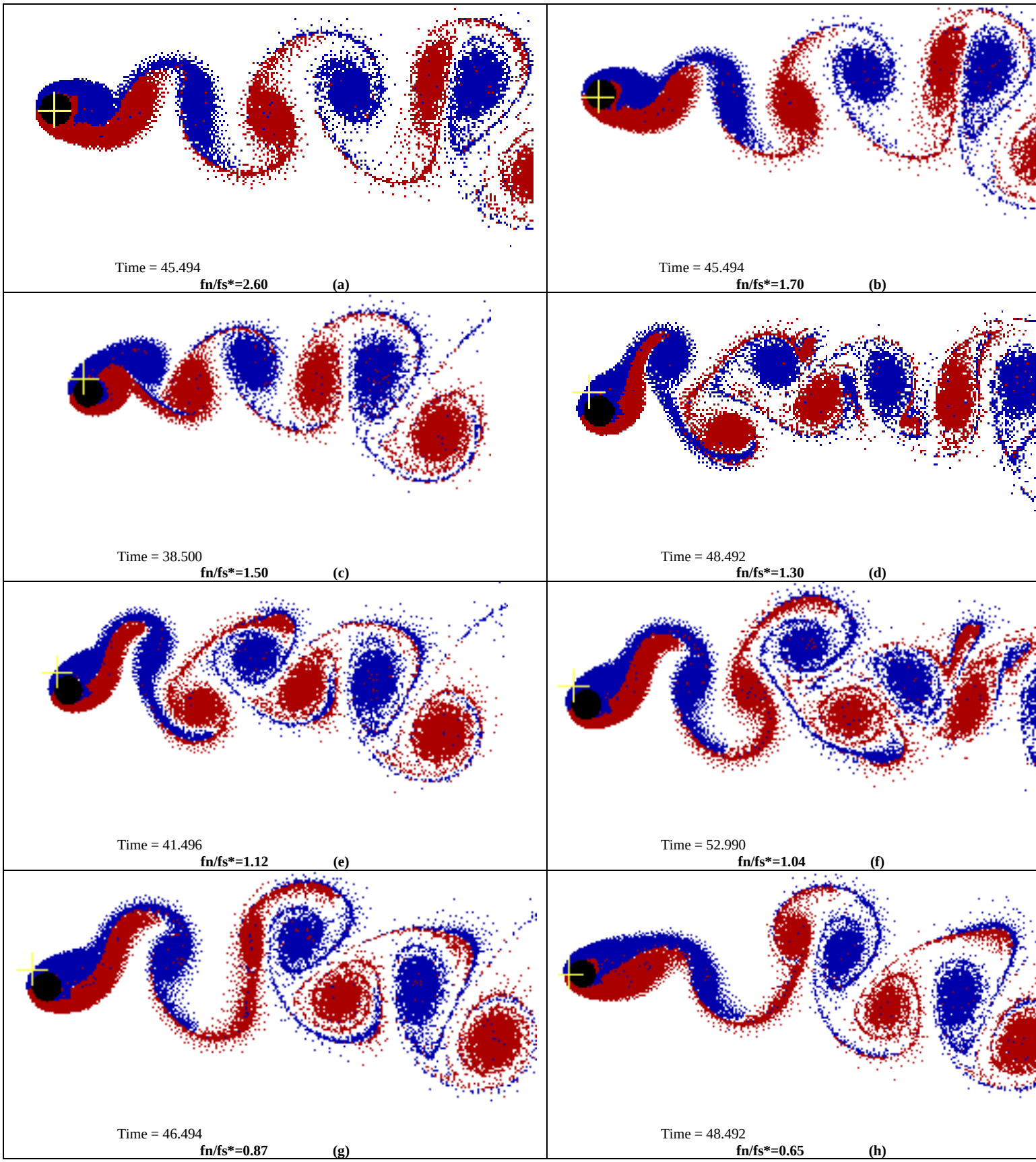


**Figure 3.9 Variation of wake structure as function of $f_n/f_s^*$ ratio for Case-3**

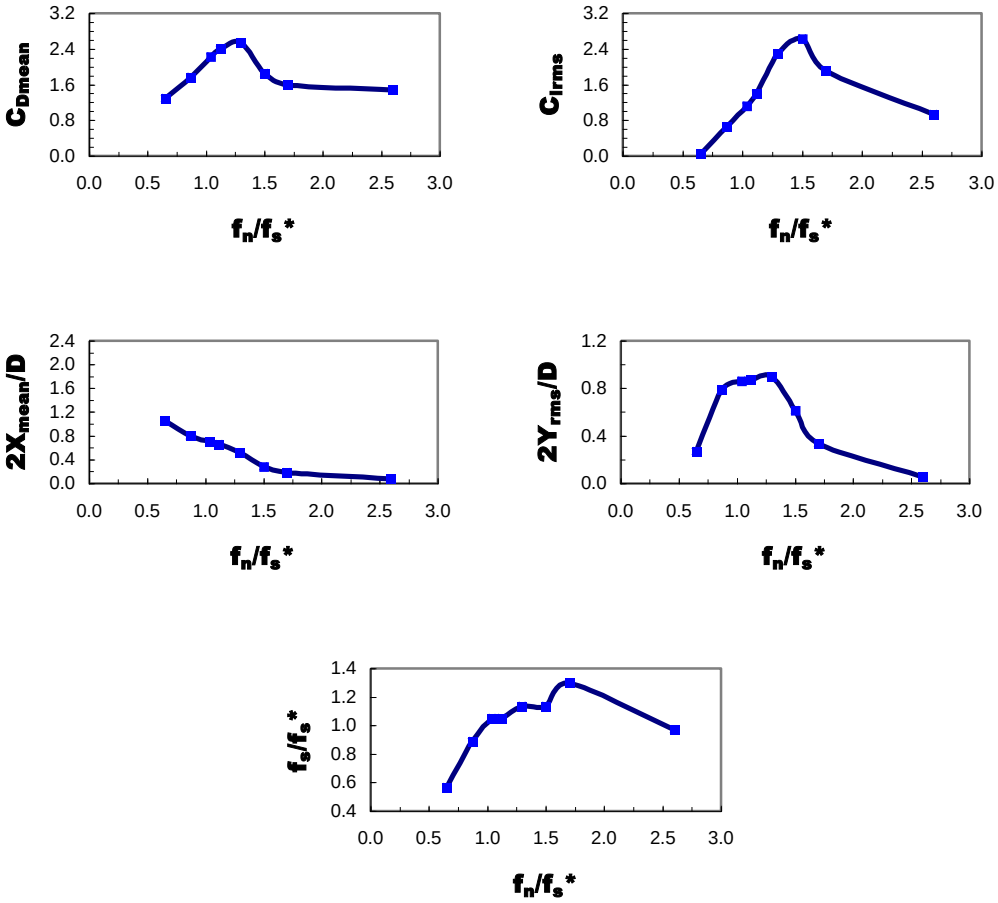


**Figure 3.10 Results for the Case-3 at Re=200 and Sg=0.01**

### 3.3.4 CASE – 4

In this case the displacement phase plot (Figure B4.5) shows us that for the $f_n/f_s$*=2.60 cylinder behave like rigid cylinder that is the displacements are negligible. Decreasing the frequency ratio, circular cylinder begins to vibrate. As approaching to the value $f_n/f_s$*=1.30 it shows a violent vibration easily seen by the time histories of $C_L$, $C_D$, Y/D and X/D values in Appendix B4 and Figure 3.11.

It is also noted that both the transverse oscillation amplitude of the cylinder and the drag coefficient reach their maximum values at the frequency ratios $f_n/f_s$*=1.30 as we found in the Case-2 where the maximum values for $C_{Dmean}$ and $2Y_{rms}/D$ is 2.46 and 0.87 respectively.

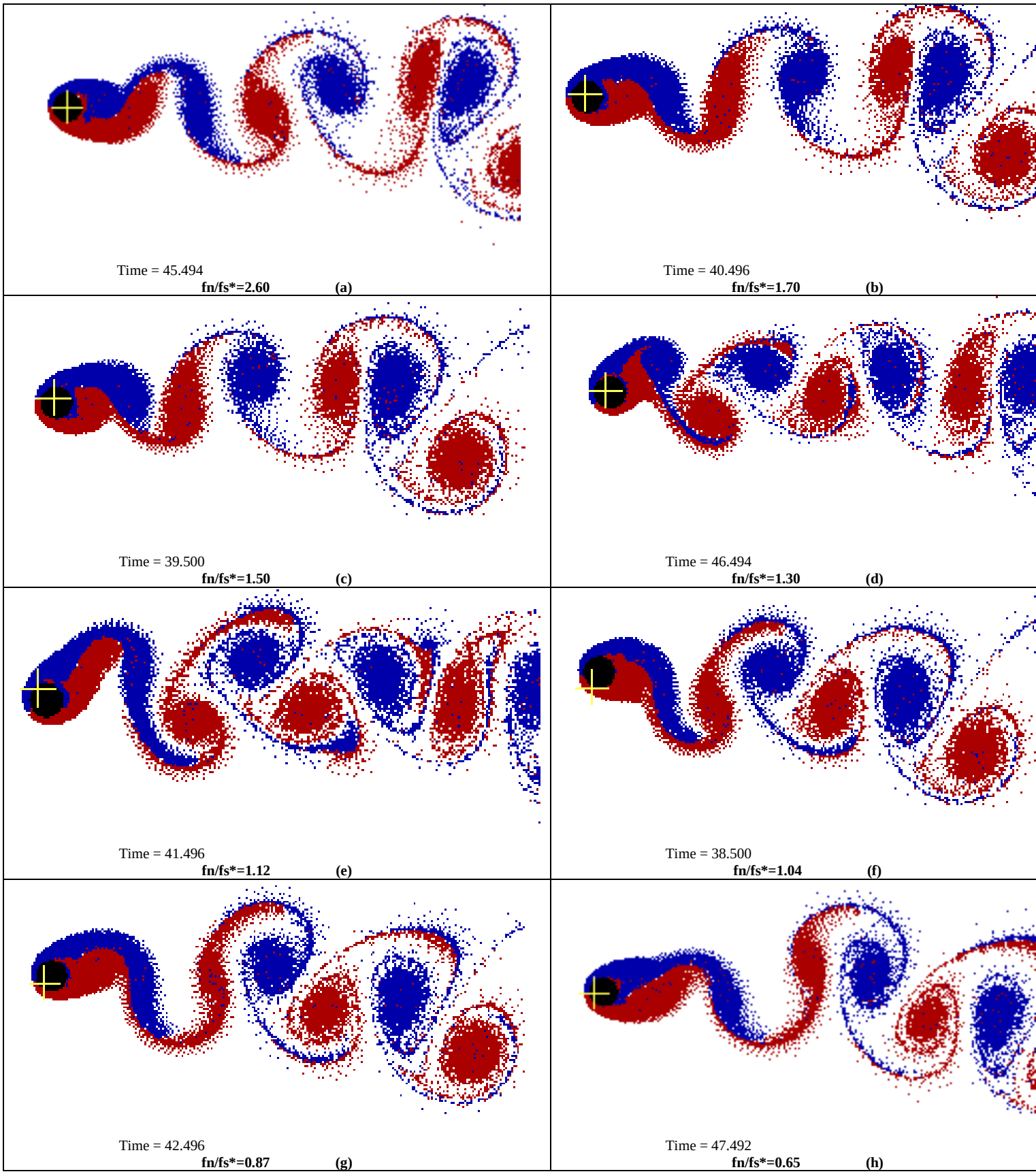


**Figure 3.11 Variation of wake structure as function of $f_n/f_s^*$ ratio for Case-4**

Similar to the Case-3, for large values of $f_n/f_s^*$ the x displacement of Case-4 tends to approach zero value and so does the y displacement (Figure 3.12).

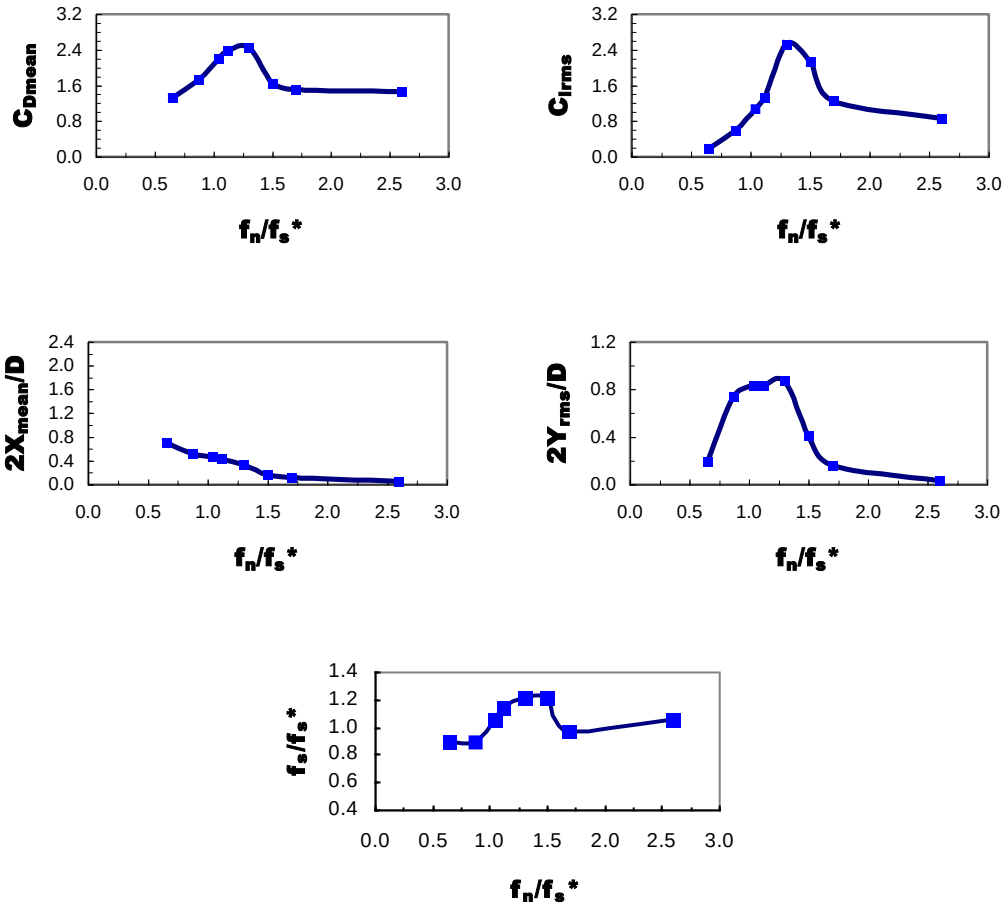


**Figure 3.12 Results for the Case-4 at Re=200 and Sg=0.01**

### 3.3.5 CASE – 5

In this case the mass ratio becomes very large and the damping parameter reaches minimum value considered in this study. The maximum values for $C_{Dmean}$ and $2Y_{rms}/D$ occur at $f_n/f_s^*=1.12$ are 2.31 and 0.80 respectively. Generally, the most violent vibration is expected to happen when the vibration frequency of the cylinder is about the same as the natural frequency of the fluid-structure system. In Zhou's study the maximum values for the characteristics occurred at $f_n/f_s^*=1.04$.

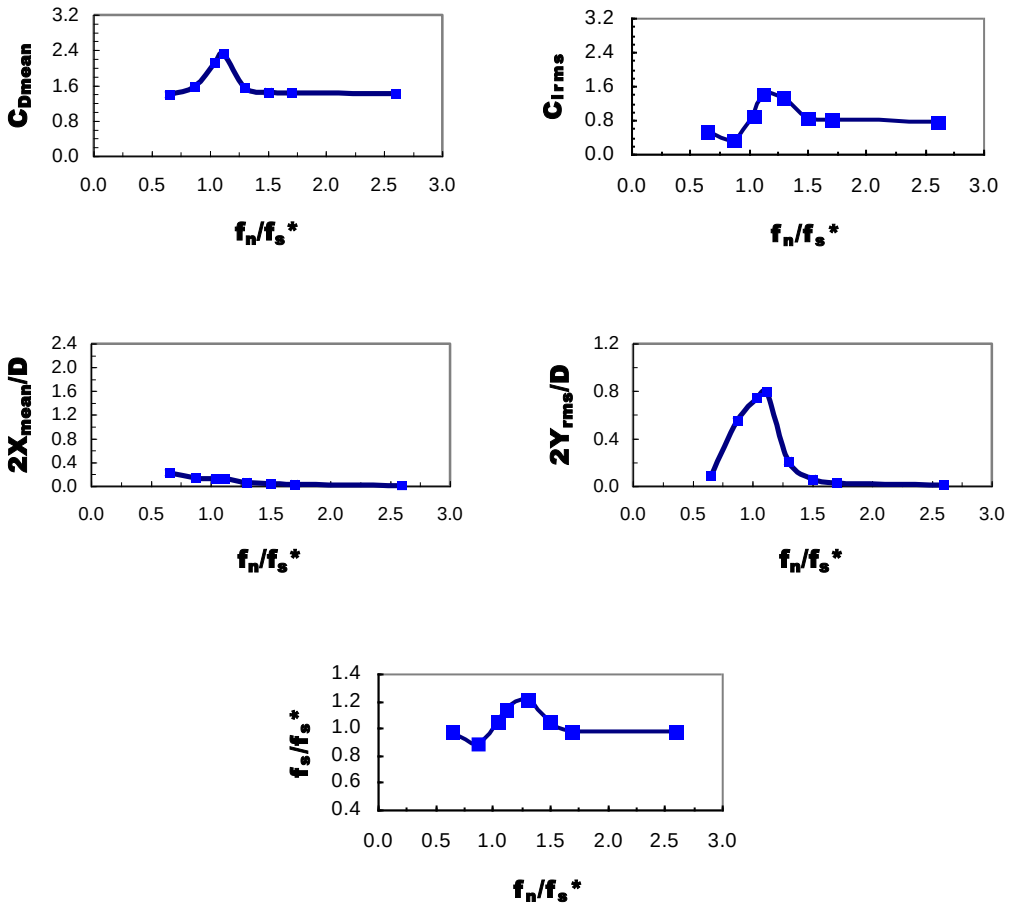


**Figure 3.13 Results for the Case-5 at Re=200 and Sg=0.01**

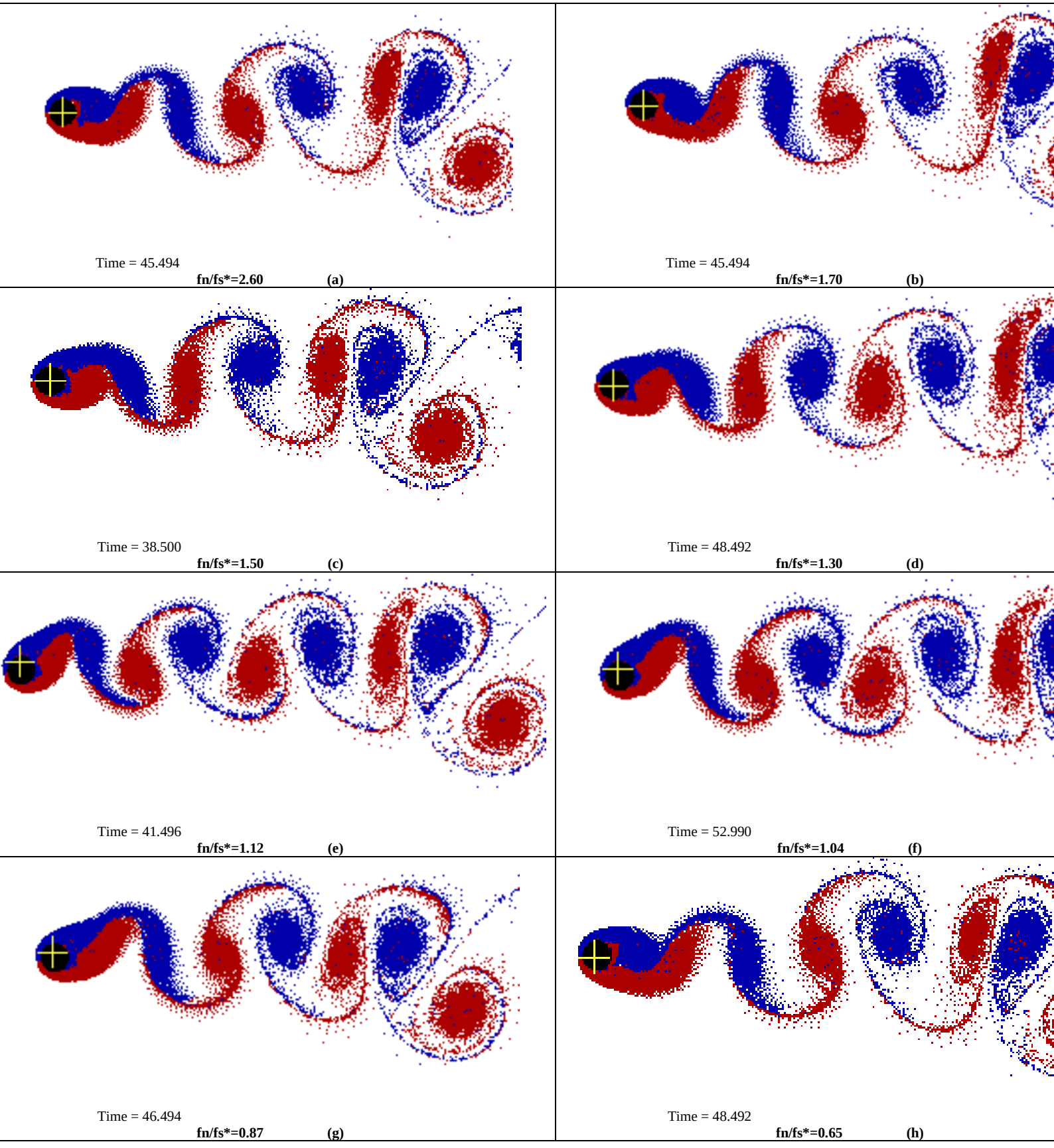


**Figure 3.14 Variation of wake structure as function of $f_n/f_s^*$ ratio for Case-5**

In Figure 3.14 we see the comparison of the vortex pattern in the wake of the elastically mounted circular cylinder at different frequency ratios. Each vortex pattern corresponds to an instant at which lift coefficient is minimum. The comparison of transverse oscillation is given in Figure 3.15. A good agreement is found with Zhou's [2] study. Time histories of the characteristics values, power spectrum of drag and lift coefficients and the displacement phase plots are given in Appendix B5.

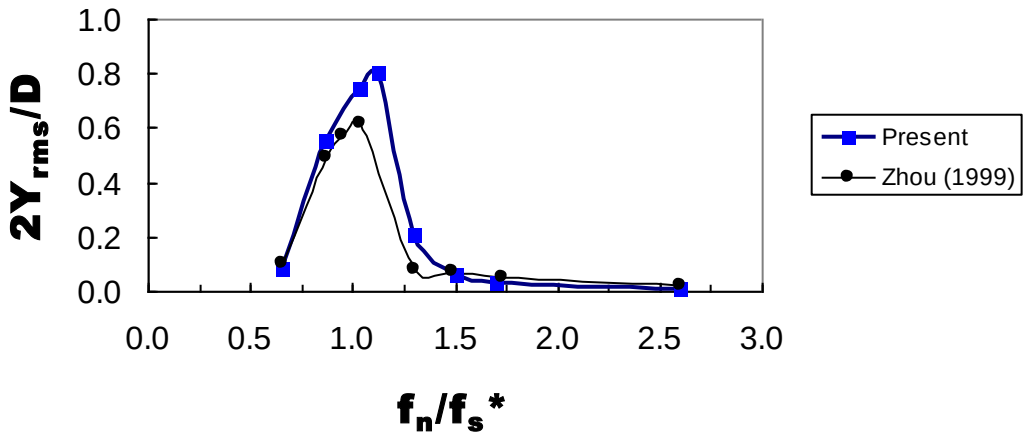


**Figure 3.15 Variation of the root mean square oscillation amplitude $2Y_{rms}/D$ as function of $f_n/f_s^*$ ratio for the Case-5**

### 3.4 Conclusions

- It is observed that the peak bands of the $C_{Dmean}$, $2Y_{rms}/D$ and $C_{lrms}$ are much wider for the M*=1, 1.5, 2, 3 cases than for the M*=10 case. In other words, a lighter structure has a wider resonance band.

- The vibration amplitude of the cylinder obviously decreases as M* increases, i.e. a heavier structure have less violent vibration. (Table 3.2)

The comparison of the all cases with the various frequency ratios is given in Figure 3.16.

- All the characteristic values tend to decrease with increasing the mass ratio M*. As also seen from the Figure 3.16 that the locking on region is changing with changing the mass ratio.

**Table 3.2 Maximum values of $C_{Dmean}$ and $2Y_{rms}/D$ corresponding to different mass ratios.**

| M* | Maximum $C_{Dmean}$ | Maximum 2Yrms/D |
|---|---|---|
| 1 | 2.60 | 0.97 |
| 1.5 | 2.56 | 0.92 |
| 2 | 2.54 | 0.90 |
| 3 | 2.46 | 0.87 |
| 10 | 2.31 | 0.80 |

- As fn/fs* increases, the mean value of the drag coefficient approaches a constant value 1.43, and the root mean square of the lift coefficient 0.72, which is the value for the rigid cylinder.Furthermore, the value of Yrms/D and Xmean/D tends to zero.

**Table 3.3 Characteristic values corresponding to M* for the fn/fs*=2.60**

| M* | $C_{Dmean}$ | $C_{lrms}$ | $Y_{rms}/D$ | $X_{mean}/D$ |
|---|---|---|---|---|
| 1 | 1.47 | 1.05 | 0.0549 | 0.0745 |
| 1.5 | 1.49 | 0.99 | 0.0360 | 0.0502 |
| 2 | 1.48 | 0.93 | 0.0263 | 0.0375 |
| 3 | 1.46 | 0.86 | 0.0165 | 0.0247 |
| 10 | 1.42 | 0.75 | 0.0045 | 0.0071 |

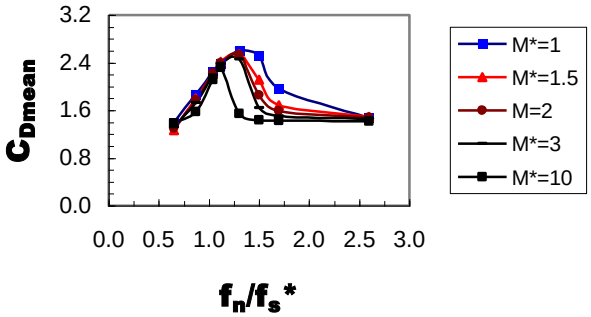


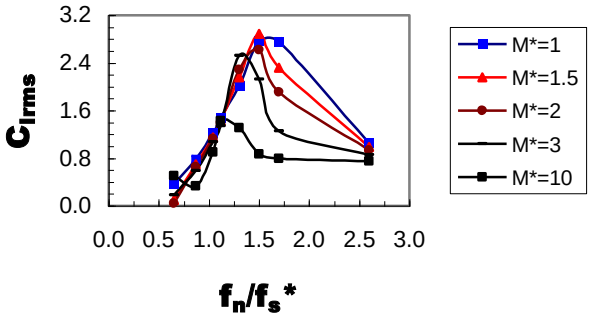


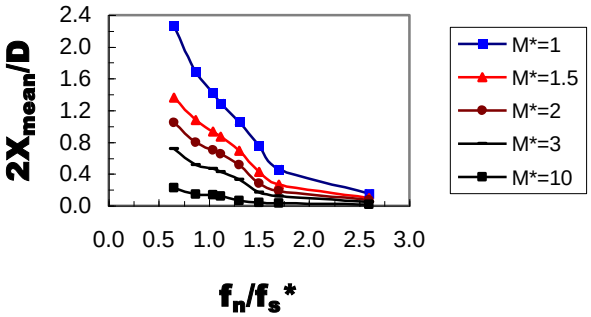


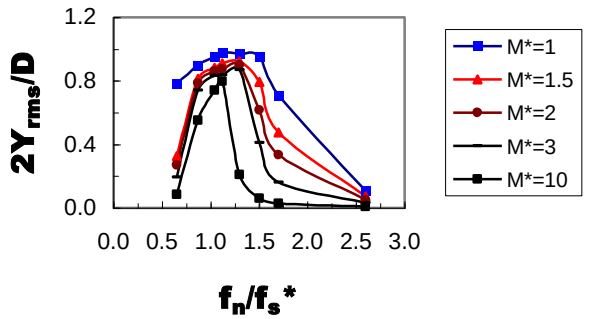


**Figure 3.16 Characteristic values for the oscillating circular cylinder for all cases**

## REFERENCES


**[1] Sarpkaya, T.,** 1979. Vortex-Induced Oscillations, *Journal of Applied Mechanics*, **46**, 241-258.

**[2] Zhou, C. Y., So, R. M. C., Lam, K.**, 1999. Vortex Induced vibrations of an elastic circular cylinder, *Journal of Fluids and Structures*, **13**, 165-189.

**[3] Zhou, C. Y., So, R. M. C.,** 2000. Fluid Dmaping of an elastic cylinder in a cross-flow, *Journal of Fluids and Structures*, **14**, 303-322.

**[4] Cheer, A. Y.,** 1983. Numerical Study of incompressible slightly viscous flow past blunt bodies and airfoils, *SIAM Journal on Scientific and Statistical Computing*, **4**, 685-705.

**[5] Cheer, A. Y.,** 1989. Unsteady separated wake behind an impulsively started cylinder in slightly viscous fluid, *Journal of Fluid Mechanics*, **201**, 485-505.

**[6] Stansby, P. K.**, **Smith, P. A.,** 1983. Simulation of flows around cylinders by a Langrangian vortex scheme, *Applied Ocean Research*, **5**, 167-178.

**[7] Smith, P. A.**, **Stansby, P. K.,** 1988. Impulsively started flow around a circular cylinder by the vortex method, *Journal of Fluid Mechanics*, **194**, 45-77.

**[8] Smith, P. A.**, **Stansby, P. K.,** 1989. Postcritical flow around a circular cylinder by the vortex method, *Journal of Fluids and Structures*, **35**, 275-292.

**[9] Baldwin, B. S.**, **Lomax, H.,** 1978. Thin layer approximation and algebraic model for separated turbulent flows, *AIAA paper AIAA*, 78-257.

**[10] Slaouti, A.**, **Stansby, P. K.,** 1992. Flow around two circular cylinders by the random-vortex method, *Journal of Fluids and Structures*, **6**, 641-670.

**[11] Blevins, R. D.**, 1989. Application of the discrete vortex method to fluid-structure interaction in Flow-Induced Vibration, *ASME Journal of Pressure Vessel Technology 1991*, **113**, 437-445.

**[12] Meneghini, J. R., Bearman, P. W.,** 1993. Numerical Simulation of high amplitude oscillatory-flow about a circular cylinder using a discrete vortex method, *AIAA paper AIAA*, 93-328.

**[13] Akbari, M., Price S. J.,** 1997. Simulation of the incompressible viscous cross-flow around an oscillating circular cylinder via the random vortex method, *(ASME) AD-Vol. 53.1, Fluid-Structure Interaction, Aeroelasticity, Flow-Induced Vibration and Noise*, Vol. I, 21-32.

**[14] Matsumoto, H., Kamemoto, K., Yokoi, Y.,** 1997. Application of Advanced Vortex Method to Simulation of self-excited vibration of a circular cylinder in two dimensional uniform flow, *(ASME) AD-Vol. 53.1, Fluid-Structure Interaction, Aeroelasticity, Flow-Induced Vibration and Noise*, Vol. I, 33-40.

**[15] Kamemoto, K., Matsumoto, H., Yokoi, Y.,** 1994. On the extensive applicability of vortex methods to prediction of flow induced vibration problems, *Proceedings 6$^{th}$ International Conference on flow induced vibration*, 205-212.

**[16] Kamemoto, K.,** 1995. On attractive features of the vortex methods, *Computational Fluid Dynamics Review*, John Wiley & Sons, 334-353.

**[17] Cetiner, O.,** 1992. Vortex-Induced Oscillations of an elastically mounted circular cylinder, *M.Sc. Thesis*, Istanbul Technical University.

**[18] Chorin, A. J.,** 1973. Numerical Study of slightly viscous flow, *Journal of Fluid Mechanics*, **57**, 785-796.

**[19] Young, J. A.,** 1989. Viscous flow around vortex shedding flowmeters: A discrete vortex model, *Ph.D. Thesis*, Faculty of Engineering, University of London.

**[20] Roache, P. J.,** 1972. Computational Fluid Dynamics, Hermosa Publishers.

**[21] Christiansen, J. P.,** 1973. Numerical Simulation of hydrodynamics by the method of point vortices, *Journal of Computational Physics*, **13**, 363-379.

## APPENDIX A1

## DISCRETIZATION OF POISSON'S EQUATIONS

The Poisson's equation;

$$\nabla^2\psi = \frac{\partial^2\psi}{\partial x^2} + \frac{\partial^2\psi}{\partial y^2} = -\frac{\Gamma}{A} \tag{A1.1}$$

is written in finite difference form according to the Eularian concept of discretising the flow field onto a mesh. For constant mesh spacing in x direction, the second order central differencing is used:

$$f_i^{"} = \frac{f_{i-1} - 2f_i^2 + f_{i+1}}{\Delta x_i^2} + O(\Delta x_i)^3 \tag{A1.2}$$

for unequal, expanding mesh spacing in y direction, definition of mesh intervals is given as

$$\Delta y_j = y_{j+1} - y_j \tag{A1.3}$$

$$\Delta y_{j-1} = y_j - y_{j-1} \tag{A1.4}$$

and the ratio of these is

$$s = \frac{\Delta y_j}{\Delta y_{j+1}} \tag{A1.5}$$

The Taylor series expansion of the function f about j are written to determine the values. $f_{j-1}$ and $f_{j+1}$. It becomes then possible to eliminate the $f_j^{'}$. Using the definitions above [(A1.3), (A1.4),(A1.5)], a second order expression for $f_j^{"}$ is obtained as

$$f_j^{"} = \frac{2s}{s+1}\frac{sf_{j-1} - (1+s)f_j + f_{j+1}}{\Delta y_j^2} + O(\Delta y_j)^3 \tag{A1.6}$$

For the right hand side of equation (A1.1) the mesh circulation is defined as

$$\Gamma_{i,j} = \omega_{i,j}\Delta x_i \frac{\Delta y_j + \Delta y_{j-1}}{2} \tag{A1.7}$$

and finally the finite difference form of Poisson's equation is

$$\frac{\psi_{i-1,j} - 2\psi_{i,j} + \psi_{i+1,j}}{\Delta x_i^2} + \frac{2s}{s+1}\frac{s\psi_{i,j-1} - (1+s)\psi_{i,j} + \psi_{i,j+1}}{\Delta y_j^2} = -\frac{2\Gamma_{i,j}}{\Delta x_i(\Delta y_j - \Delta y_{j-1})} \tag{A1.8}$$

On the other hand, the discrete Fourier transform of a function $F_j$ is considered as

$$\overline{F_k} = \sum_{j=0}^{N-1} \exp(2\pi ijk/N).F_j \qquad \text{k=0,1,...,N-1} \tag{A1.9}$$

The discrete Fourier transform and its inverse are computed with an algorithm called Fast Fourier Transform in order to reduce number of operations. Transforming the x directional contribution to (A1.8) gives

$$\begin{aligned}\overline{\psi_{i-1,j} - 2\psi_{i,j} + \psi_{i+1,j}} &= \overline{\psi_{i,j}}[\exp(-2\pi ik) - 2 + \exp(2\pi ik)] \\ &= 2\overline{\psi_{i,j}}\left[\cos\frac{2\pi k}{N} - 1\right]\end{aligned} \tag{A1.10}$$

For numbering of j and k from 1 to N, this becomes

$$\overline{\psi_{i-1,j} - 2\psi_{i,j} + \psi_{i+1,j}} = 2\overline{\psi_{i,j}}\left[\cos\frac{2\pi(k-1)}{N} - 1\right] \tag{A1.11}$$

The transformation of the Poisson's equation in full is therefore

$$\alpha_j \overline{\Psi}_{i,j+1} + \beta_j \overline{\Psi}_{i,j} + \varepsilon_j \overline{\Psi}_{i,j} = -\frac{2\overline{\Gamma}_{i,j}\Delta y_j^2}{\Delta x_i(\Delta y_j + \Delta y_{j-1})} \tag{A1.12}$$

with the coefficients

$$\alpha_j = \frac{2s}{s+1}, \qquad \beta_j = (-k^2\Delta y_j^2 - 2s), \qquad \varepsilon_j = \frac{2s^2}{s+1} \tag{A1.13}$$

and the wave number of transformation, k is defined as

$$-k^2 = 2\left[\cos\frac{2\pi(k-1)}{N} - 1\right]\frac{1}{\Delta x^2} \quad \Rightarrow \quad \text{k}=\left[\frac{2}{\Delta x}\sin\frac{\pi(k-1)}{N}\right] \qquad \text{(A1.14)}$$

The tridiagonal system of equation (A1.13) may be solved by Tridiagonal Matrix Algorithm to obtain Ψ values for the entire mesh. Then, the Fourier transform is inverted via

$$\psi_j = \sum_{k=0}^{N-1} \exp(-2\pi ijk/N)\overline{\psi}_k \qquad \text{j=0,1,...,N-1} \qquad \text{(A1.15)}$$

to give the stream function values on the mesh [17,19].

## APPENDIX A2

## SOLUTION OF DIFFUSION EQUATION

The second order expression for $f_j^{"}$ found in Appendix A1 (Equation A1.6), is used to obtain the finite difference form of the diffusion equation. The time derivation will be represented by a first order forward approximation. Thus the diffusion equation becomes

$$\omega_{i,j}^{(t+\Delta t)} = \omega_{i,j}^{t} + \upsilon\Delta t\left[\frac{\omega_{i-1,j}^{t} - 2\omega_{i,j}^{t} + \omega_{i+1,j}^{t}}{\Delta x_i^2} + \frac{2s}{s+1}\frac{s\omega_{i,j-1}^{t} - (1+s)\omega_{i+1,j}^{t} + \omega_{i,j+1}^{t}}{\Delta y_j^2}\right].\frac{1}{J} \tag{A2.1}$$

Using the definition of (A1.7) this equation above is rewritten in terms of circulation

$$\Gamma_{i,j}^{(t+\Delta t)} = \Gamma_{i,j}^{t} + \upsilon\Delta t\left[\frac{\Gamma_{i-1,j}^{t} - \Gamma_{i,j}^{t} + \Gamma_{i+1,j}^{t}}{\Delta x_i^2} + \frac{2s}{s+1}\frac{(\Delta y_j + \Delta y_{j-1})}{\Delta y_j^2}\left(\frac{s\Gamma_{i,j-1}^{t}}{(\Delta y_{j-1} + \Delta y_{j-2})} - \frac{(1+s)\Gamma_{i,j-1}^{t}}{(\Delta y_j + \Delta y_{j-1})} + \frac{\Gamma_{i,j+1}^{t}}{(\Delta y_{j+1} + \Delta y_j)}\right)\right].\frac{1}{J} \tag{A2.2}$$

Instead of solving explicitly the diffusion equation, a semi-implicit form of the equation (A2.2) is carried out for the calculations. This yields an expression for the circulation at mesh point (i,j), at time step t+Δt, in terms of the circulation at time step t, of the form

$$\left(1 - \frac{\alpha\upsilon\Delta t}{J}\Theta_\eta\right)\Gamma^{(t+\Delta t)} = \left(1 + \frac{\upsilon\Delta t}{J}\Theta_\xi + (1+\alpha)\frac{\upsilon\Delta t}{J}\Theta_\eta\right) \tag{A2.3}$$

where $\Theta_\xi$ and $\Theta_\eta$ are the difference operators and $\alpha$ ($0 \le \alpha \le 1$) controls the degree of implicitness in $\eta$ direction [17]

## APPENDIX A3

## EQUATIONS OF SPRING-MASS-DAMPER SYSTEM

In a non-inertial frame attached to the body, the equation of motion of an elastically mounted and linearly damped body of mass m is

$$m\ddot{Y} + c\dot{Y} + kY = F_{cy} + \rho V\ddot{Y} \tag{A3.1}$$

For a 2D circular cylinder, the volume V, the mass m, the damping constant c and the spring constant k per unit length may be written as

$$V = \frac{\pi D^2}{4} \tag{A3.2}$$

$$m = \frac{\rho_s \pi D^2}{4} \tag{A3.3}$$

$$c = 2m\omega_n \xi_s \tag{A3.4}$$

$$k = m\omega_n^2 = m(2\pi f_n)^2 \tag{A3.5}$$

and $F_{cy}$ being the instantaneous lift force, the equation (A3.1) takes the form of

$$\frac{\rho_s \pi D^2}{4}\ddot{Y} + 2m\omega_n \xi_s \dot{Y} + m\omega_n^2 Y = \frac{U^2 D C_L}{2\rho_s} + \frac{\rho \pi D^2}{4}\ddot{Y} \tag{A3.6}$$

$$\left(1 - \frac{\rho}{\rho_s}\right)\ddot{Y} + 2(2\pi f_n)\xi_s \dot{Y} + (2\pi f_n)^2 Y = \frac{\rho C_L}{\rho_s \pi}\frac{2U^2}{D} \tag{A3.7}$$

Normalizing the variables with the cylinder radius D/2 and the free stream velocity U, we obtain

$$\left(1 - \frac{\rho}{\rho_s}\right)\frac{2U^2}{D}\ddot{Y} + (2\pi f_n)\xi_s U\dot{Y} + (2\pi f_n)^2 \frac{D}{2}Y = \frac{\rho C_L}{\rho_s \pi}\frac{2U^2}{D} \tag{A3.8}$$

Simplifications yield

$$\left(1-\frac{\rho}{\rho_s}\right)\ddot{Y}+2\xi_s\left(\frac{\pi f_n D}{U}\right)\dot{Y}+\left(\frac{\pi f_n D}{U}\right)^2 Y=\frac{\rho}{\rho_s}\frac{C_L}{\pi} \tag{A3.9}$$

The mass ratio $\rho/\rho_s$, non dimensionalized frequency $f_nD/U$ and the damping ratio $\xi_s$ form the set of parameters used in this study. When we compare the parameters which used in Zhou's report [15];

$$M^* = m/\rho D^2 \quad \Rightarrow \quad M^* = \left(\rho_s \big/ \rho\right)\left(\frac{\pi}{4}\right) \quad \Rightarrow \quad \rho \big/ \rho_s = \frac{1}{M^*}\frac{\pi}{4} \tag{A3.10}$$

$$\alpha=\xi_s \tag{A3.11}$$

$$Sg = 8\pi^2 St^{*2}\alpha M^* \quad \Rightarrow \quad \alpha=\xi_s = \frac{Sg}{8\pi^2 St^{*2} M^*} \tag{A3.12}$$

$$St^* = f_s^* D/U_\infty \tag{A3.13}$$

$$1/V_r = f_n D/U_\infty \tag{A3.14}$$

$$\frac{f_n}{f_s^*} = \frac{1}{St^* V_r} \tag{A3.15}$$

So the equation of motion depends on three parameters, M*, $\alpha$, $f_n/f_s$*.

**APPENDIX B1**

**TIME HISTORIES OF LIFT COEFFICIENT, DRAG COEFFICIENT, TRANSVERSE OSCILLATION AND STREAMWISE OSCILLATION, POWER SPECTRUM OF LIFT AND DRAG COEFFICIENTS, DISPLACEMENT PHASE PLOT FOR THE CASE M*=1, Sg=0.01**

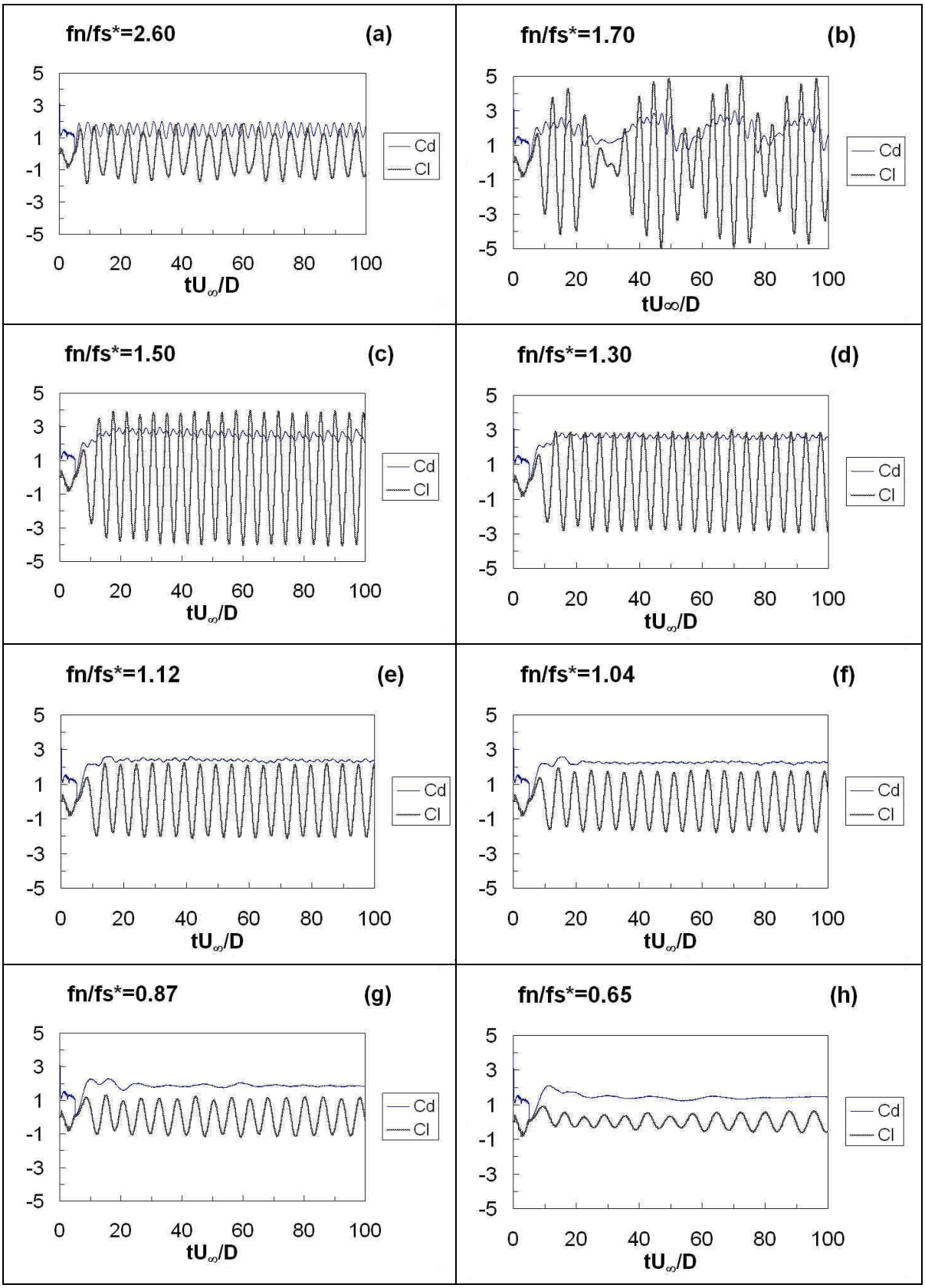


**Figure B1.1 Time histories of $C_D$ and $C_L$ coefficients with various $f_n/f_s$* ratios for the case Sg=0.01 and M*=1**

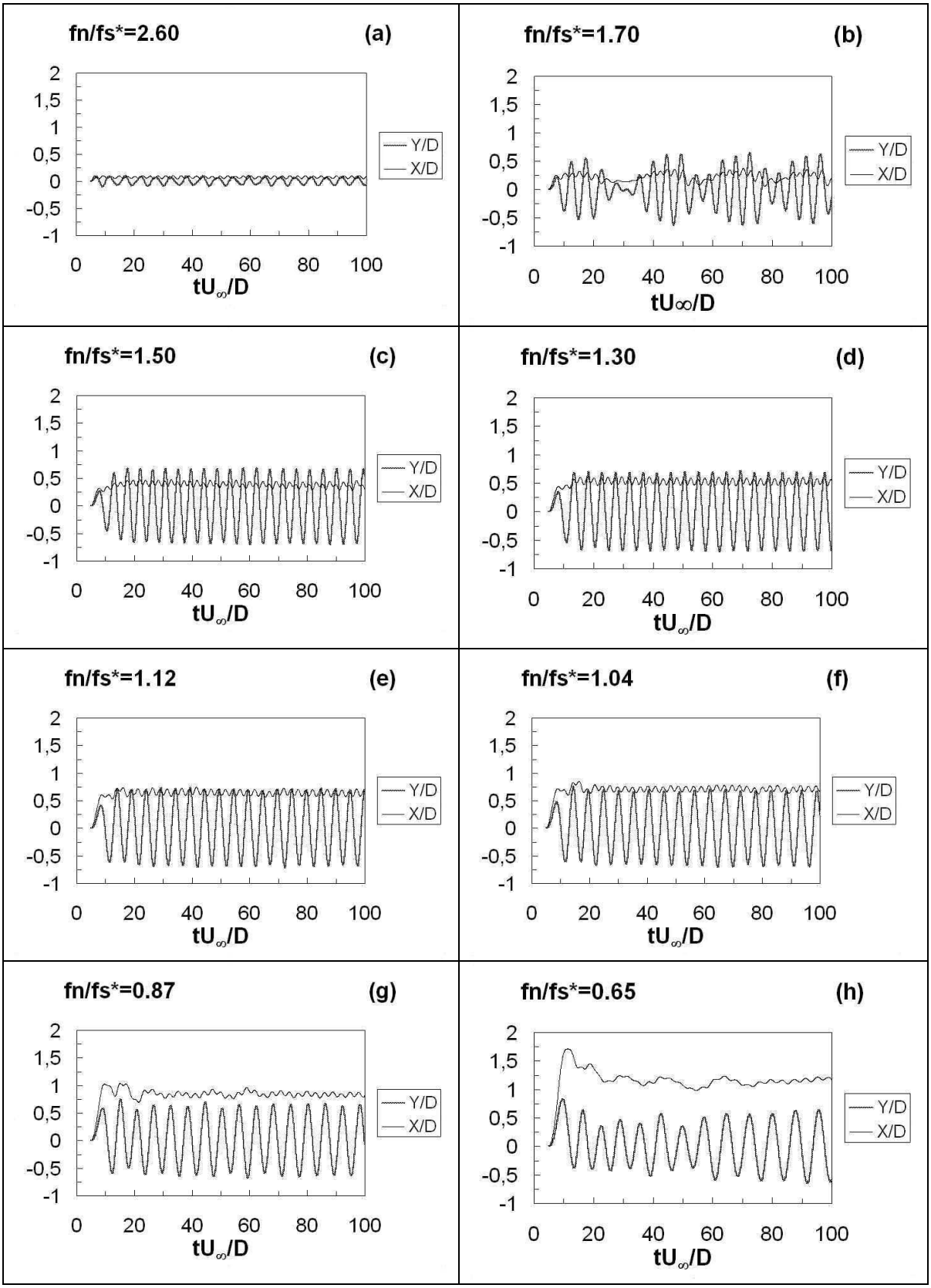


**Figure B1.2 Time histories of Displacements with various $f_n/f_s$* ratios for the case Sg=0.01 and M*=1**

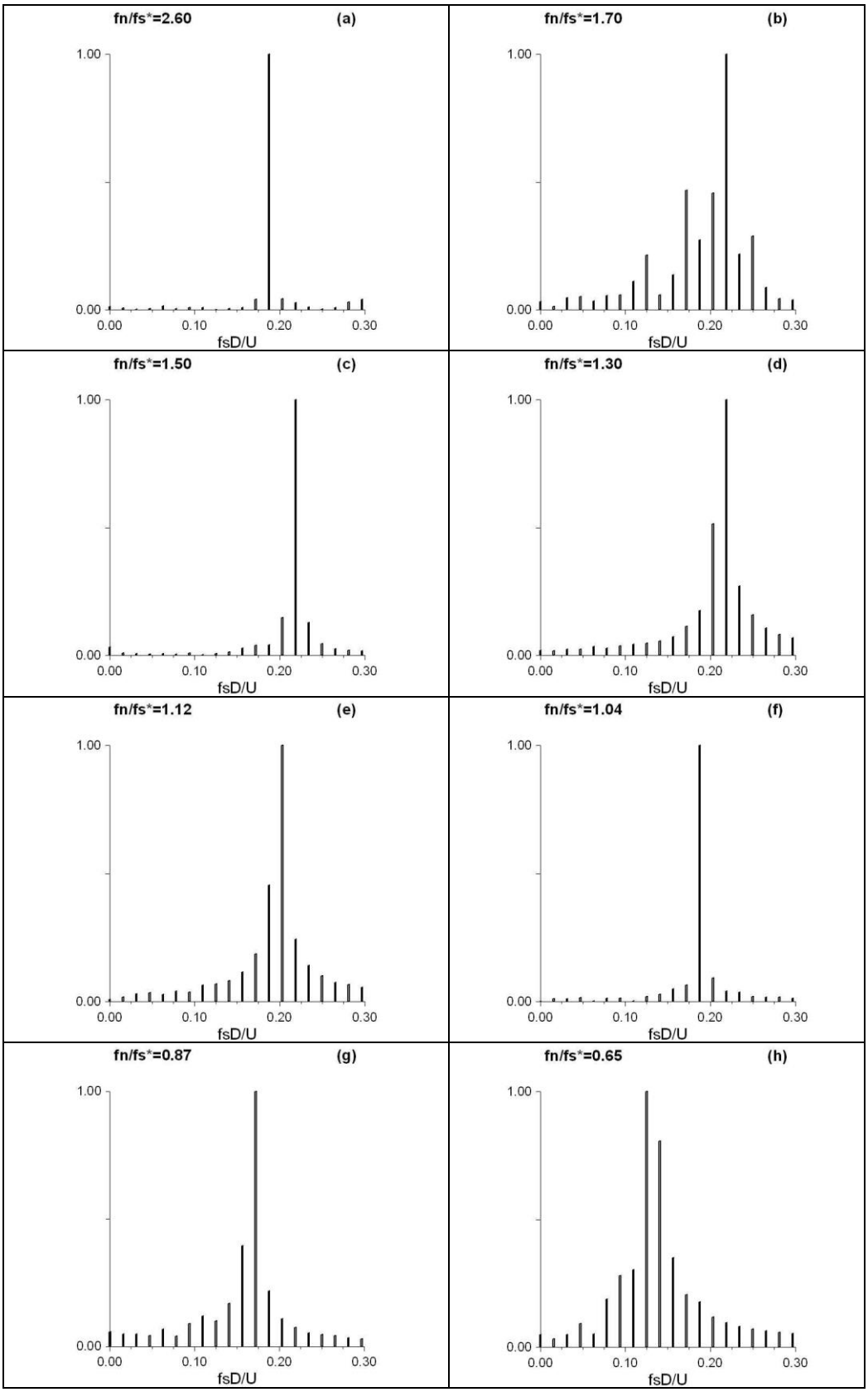


**Figure B1.3 Power Spectrum of $C_L$ oscillations with various $f_n/f_s$* ratios for the case Sg=0.01 and M*=1**

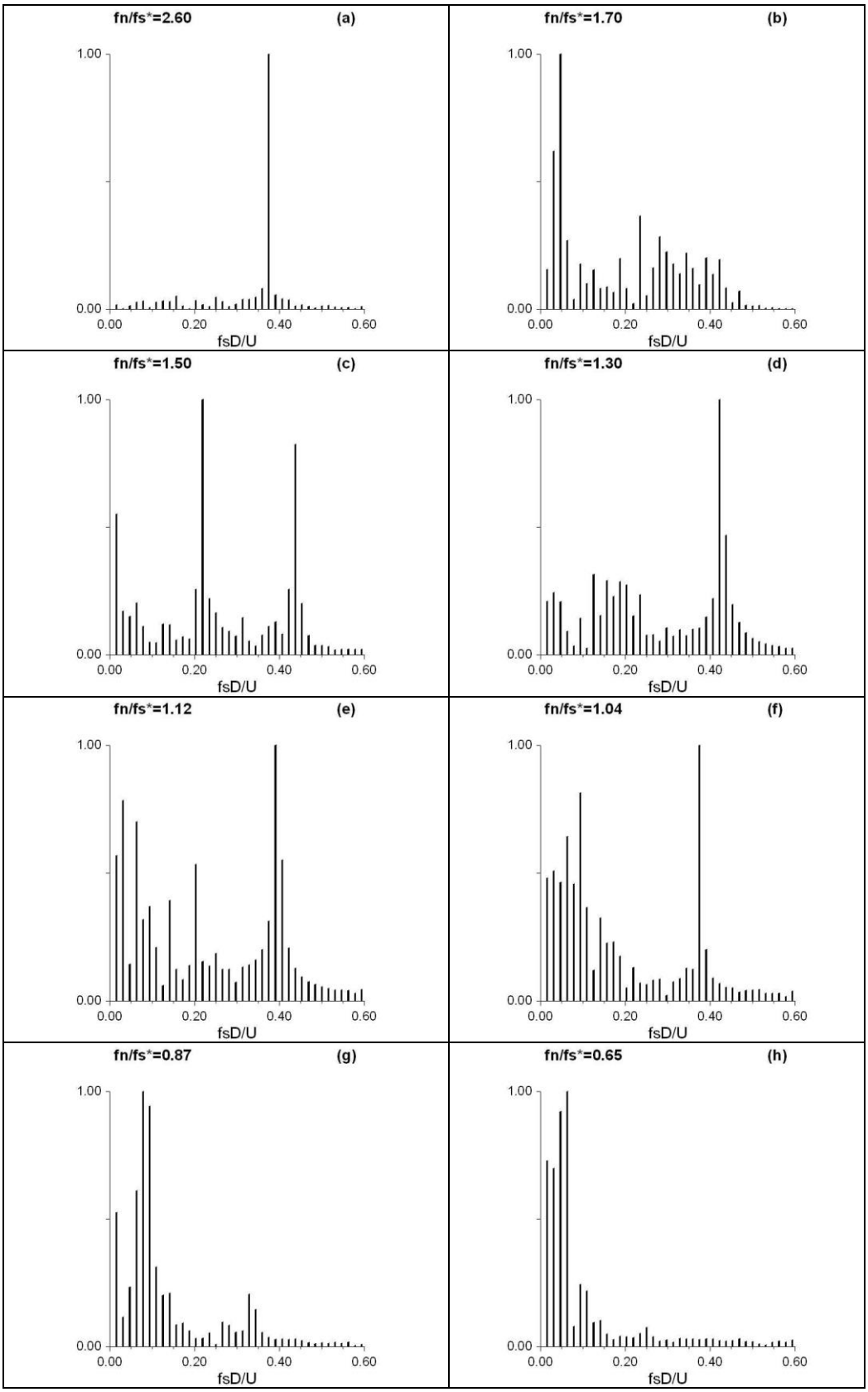


**Figure B1.4 Power Spectrum of $C_D$ oscillations with various $f_n/f_s$* ratios for the case Sg=0.01 and M*=1**

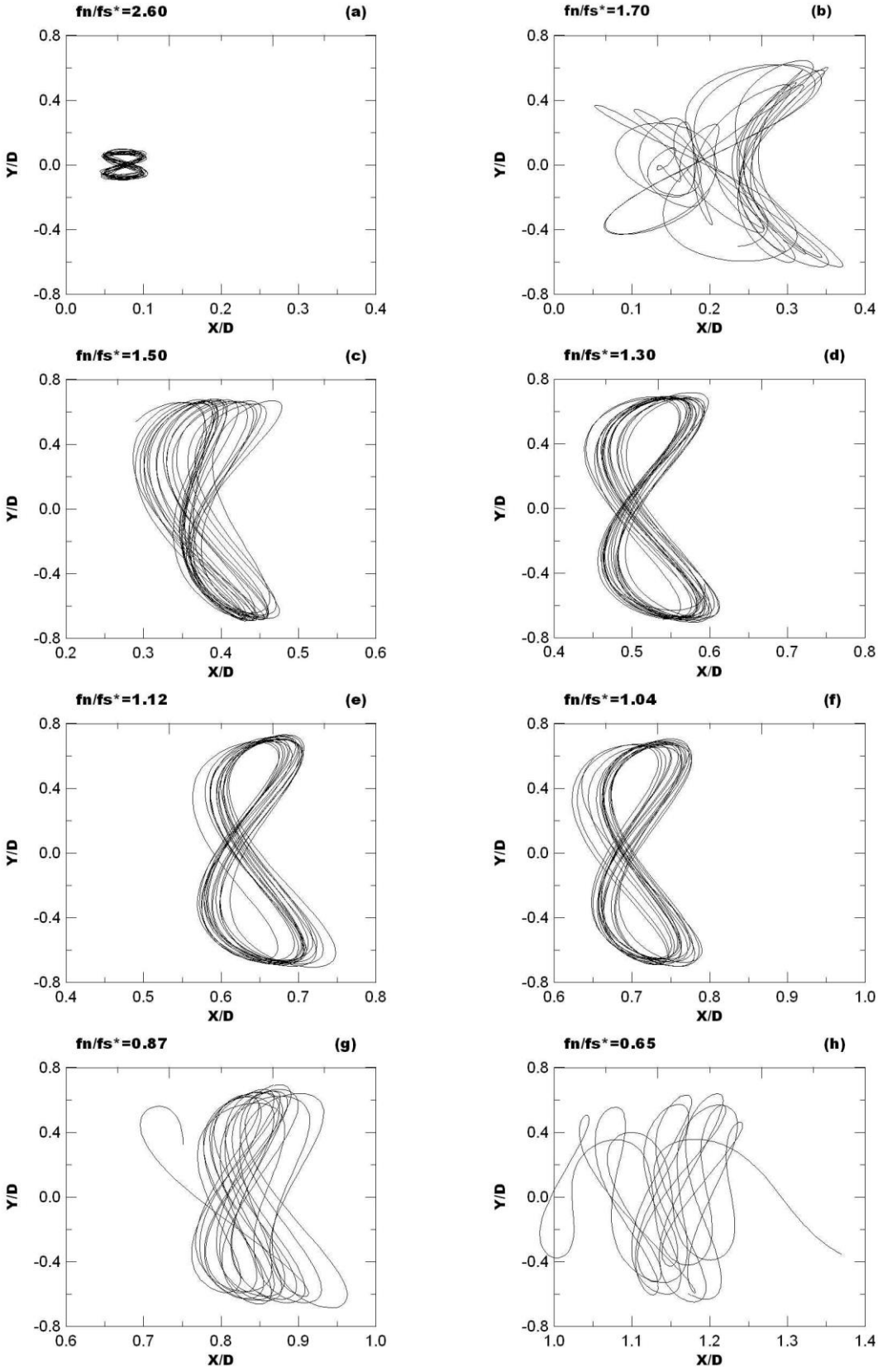


**Figure B1.5 Displacement Phase plots with various $f_n/f_s$* ratios for the case with Sg=0.01 and M*=1**

**APPENDIX B2**

**TIME HISTORIES OF LIFT COEFFICIENT, DRAG COEFFICIENT, TRANSVERSE OSCILLATION AND STREAMWISE OSCILLATION, POWER SPECTRUM OF LIFT AND DRAG COEFFICIENTS, DISPLACEMENT PHASE PLOT FOR THE CASE M*=1.5, Sg=0.01**

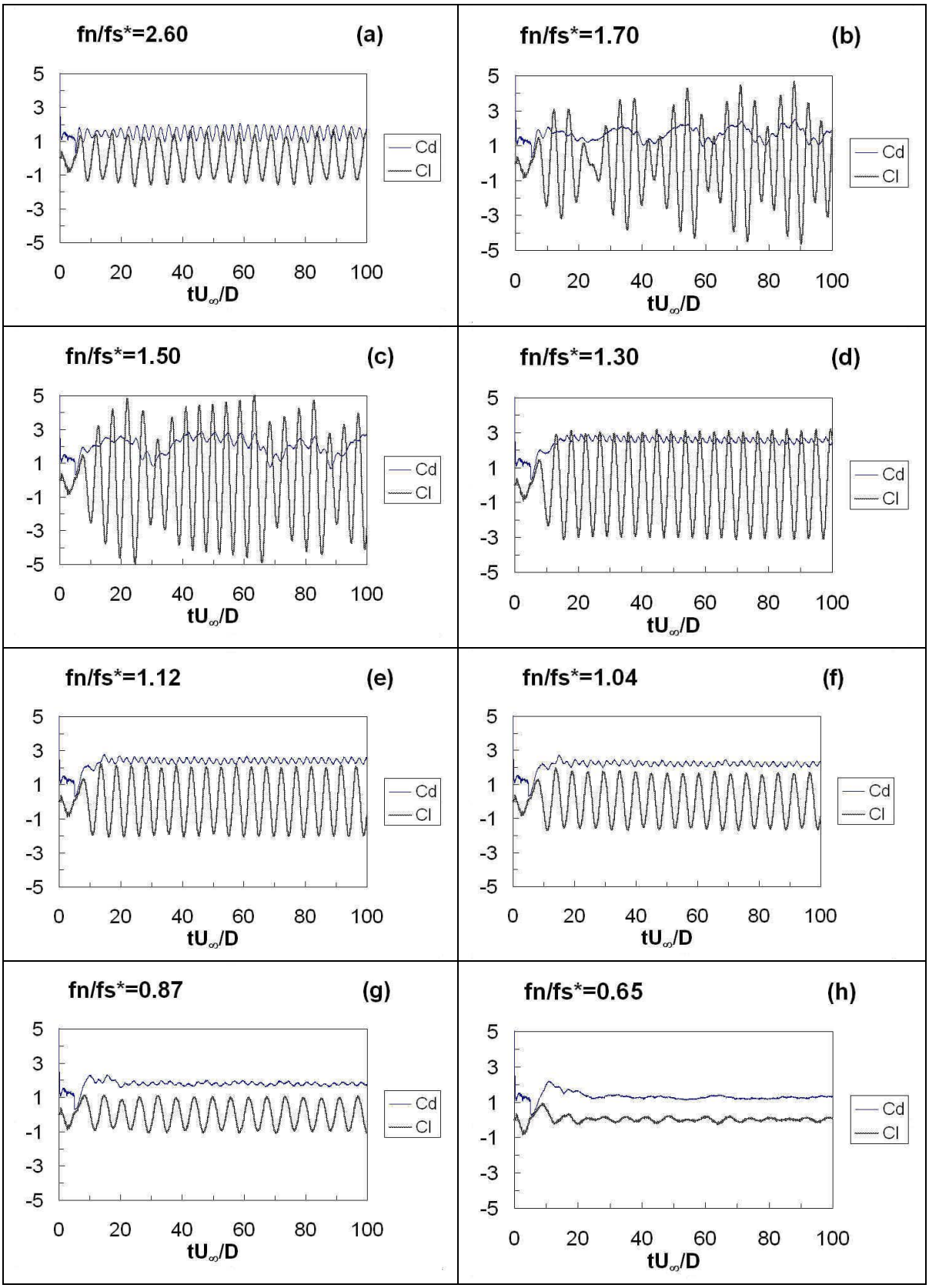


**Figure B2.1 Time histories of $C_D$ and $C_L$ coefficients with various $f_n/f_s$* ratios for the case Sg=0.01 and M*=1.5**

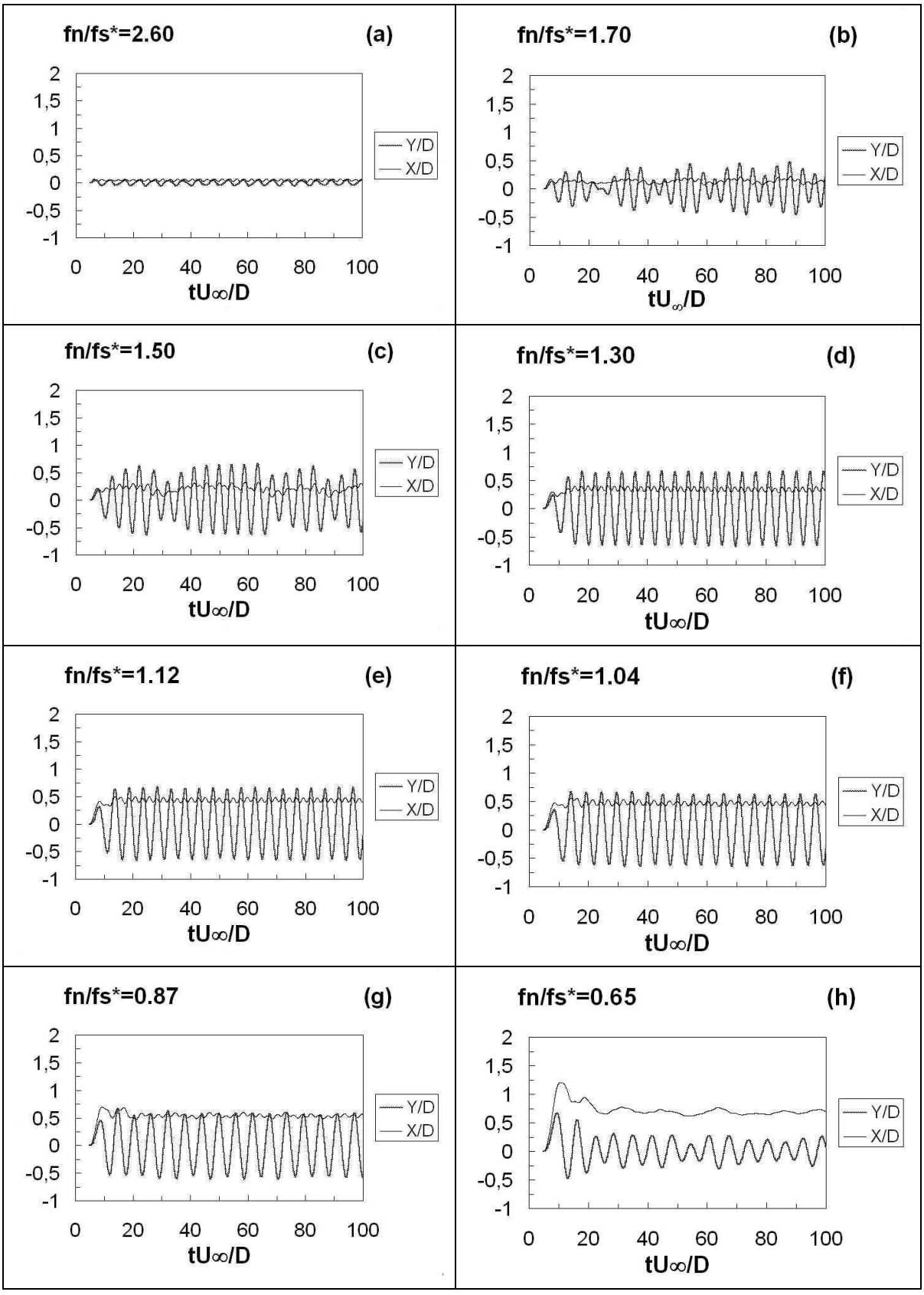


**Figure B2.2 Time histories of Displacements with various $f_n/f_s$* ratios for the case Sg=0.01 and M*=1.5**

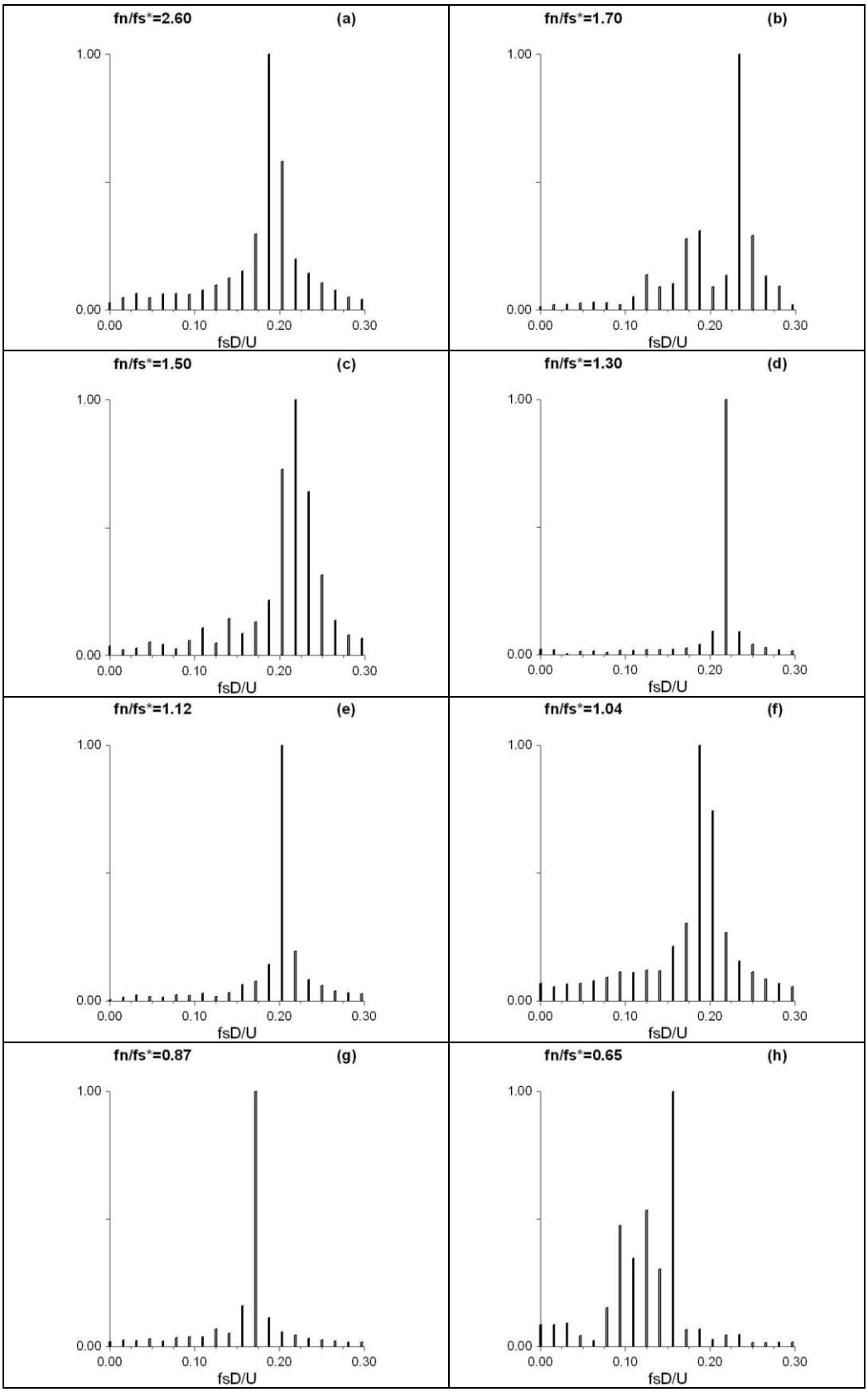


**Figure B2.3 Power Spectrum of $C_L$ oscillations with various $f_n/f_s$* ratios for the case Sg=0.01 and M*=1.5**

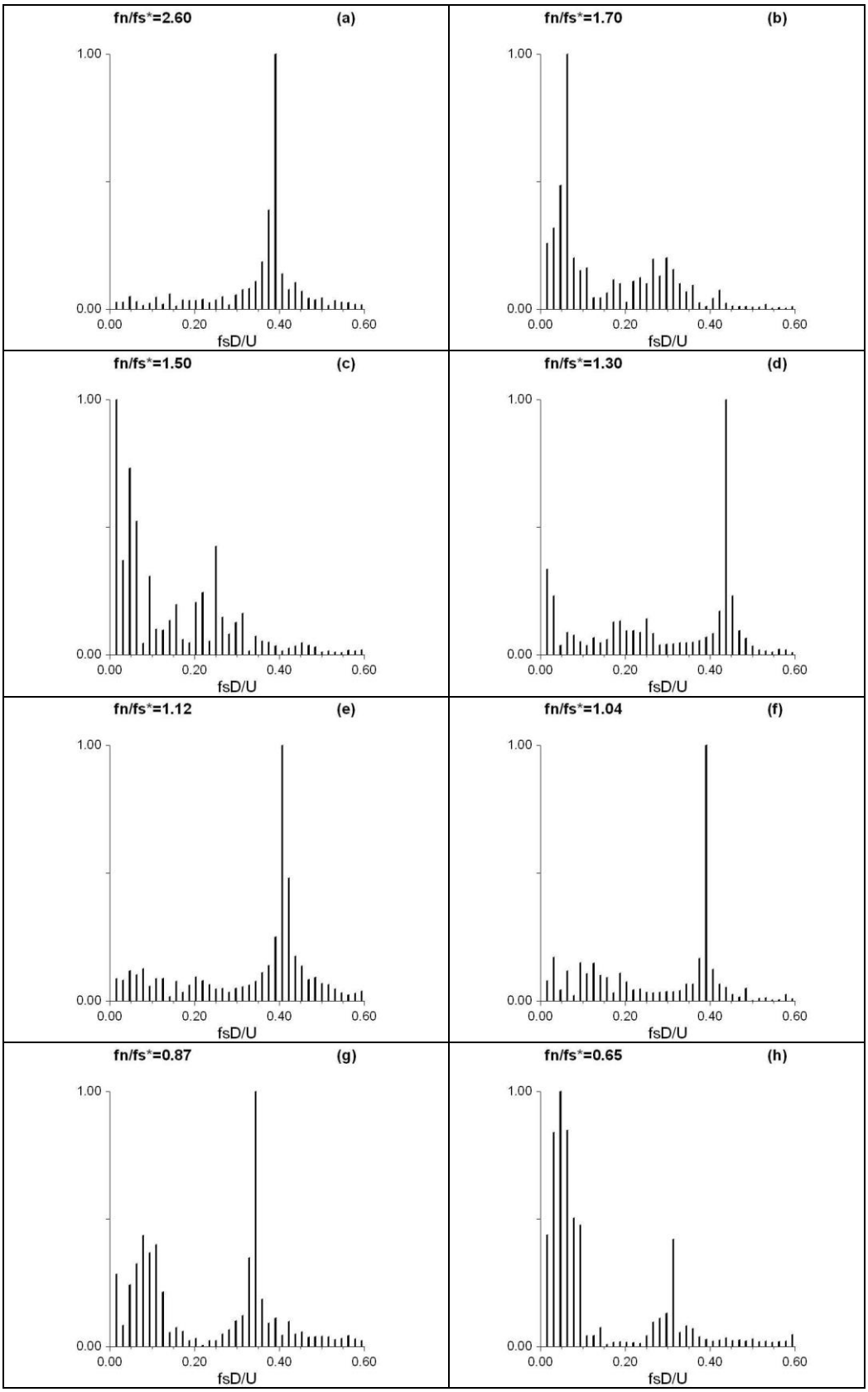


**Figure B2.4 Power Spectrum of $C_D$ oscillations with various $f_n/f_s$* ratios for the case Sg=0.01 and M*=1.5**

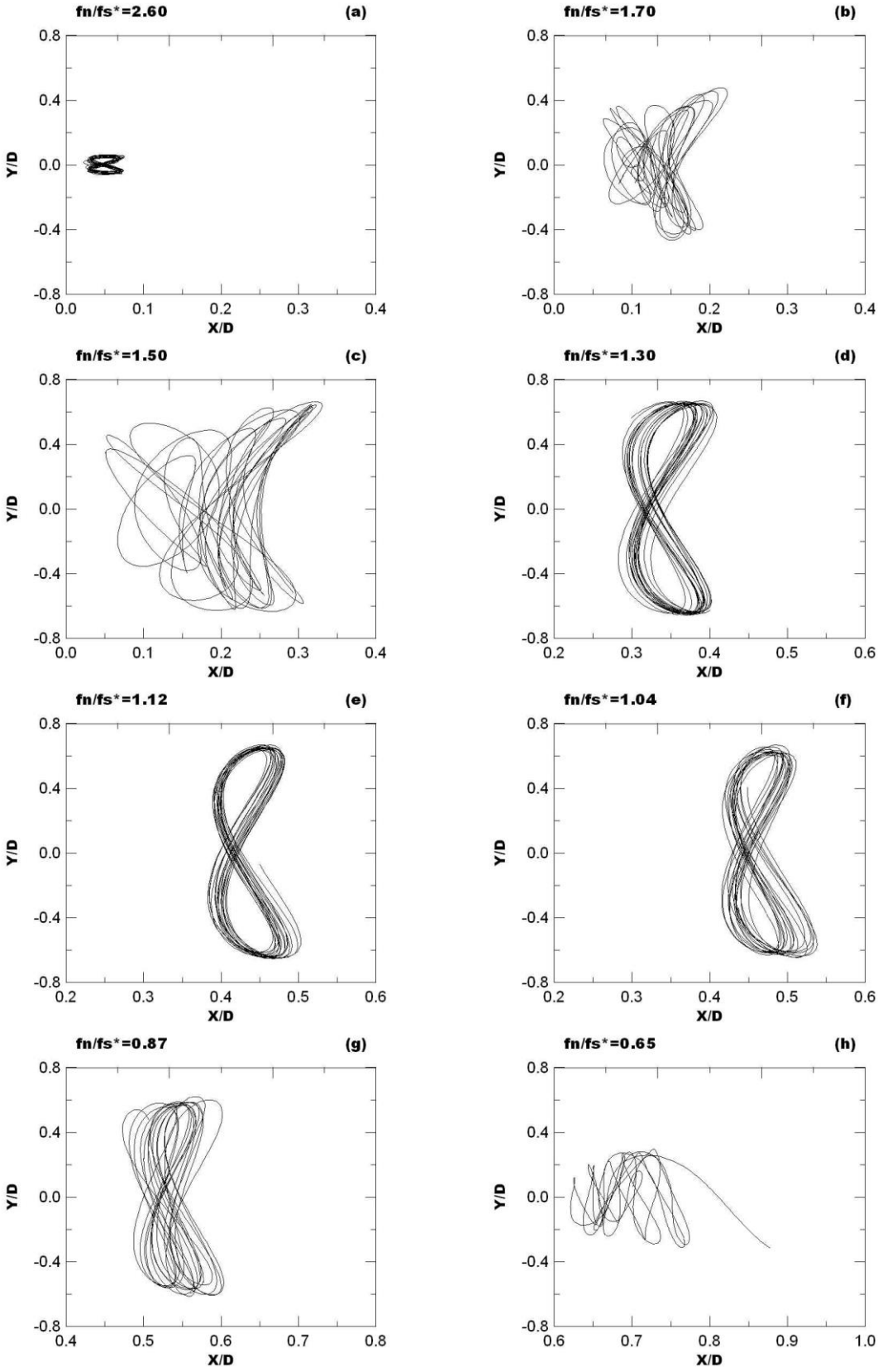


**Figure B2.5 Displacement Phase plots with various $f_n/f_s$* ratios for the case with Sg=0.01 and M*=1.5**

**APPENDIX B3**

**TIME HISTORIES OF LIFT COEFFICIENT, DRAG COEFFICIENT, TRANSVERSE OSCILLATION AND STREAMWISE OSCILLATION, POWER SPECTRUM OF LIFT AND DRAG COEFFICIENTS, DISPLACEMENT PHASE PLOT FOR THE CASE M*=2, Sg=0.01**

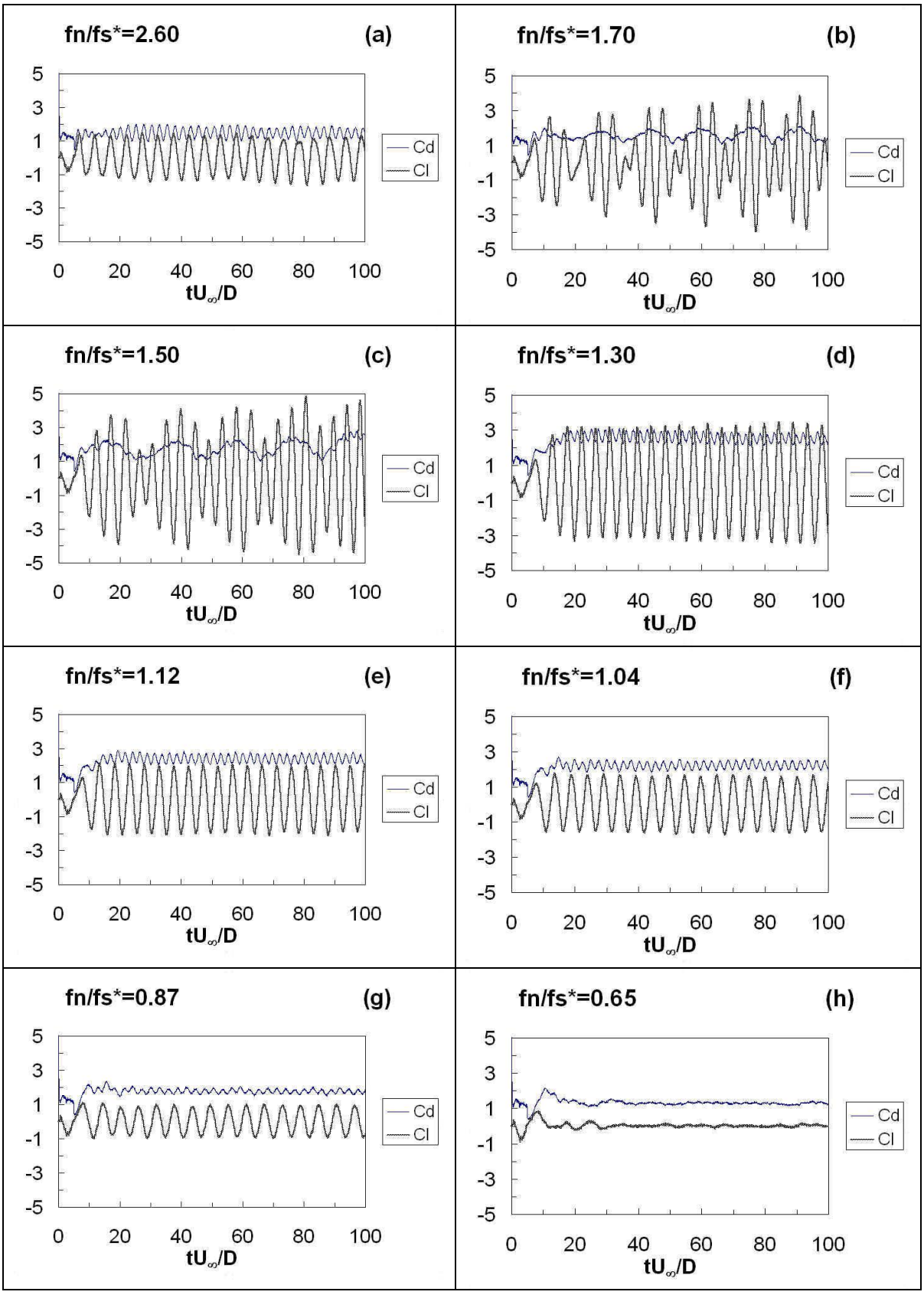


**Figure B3.1 Time histories of $C_D$ and $C_L$ coefficients with various $f_n/f_s^*$ ratios for the case Sg=0.01 and M*=2**

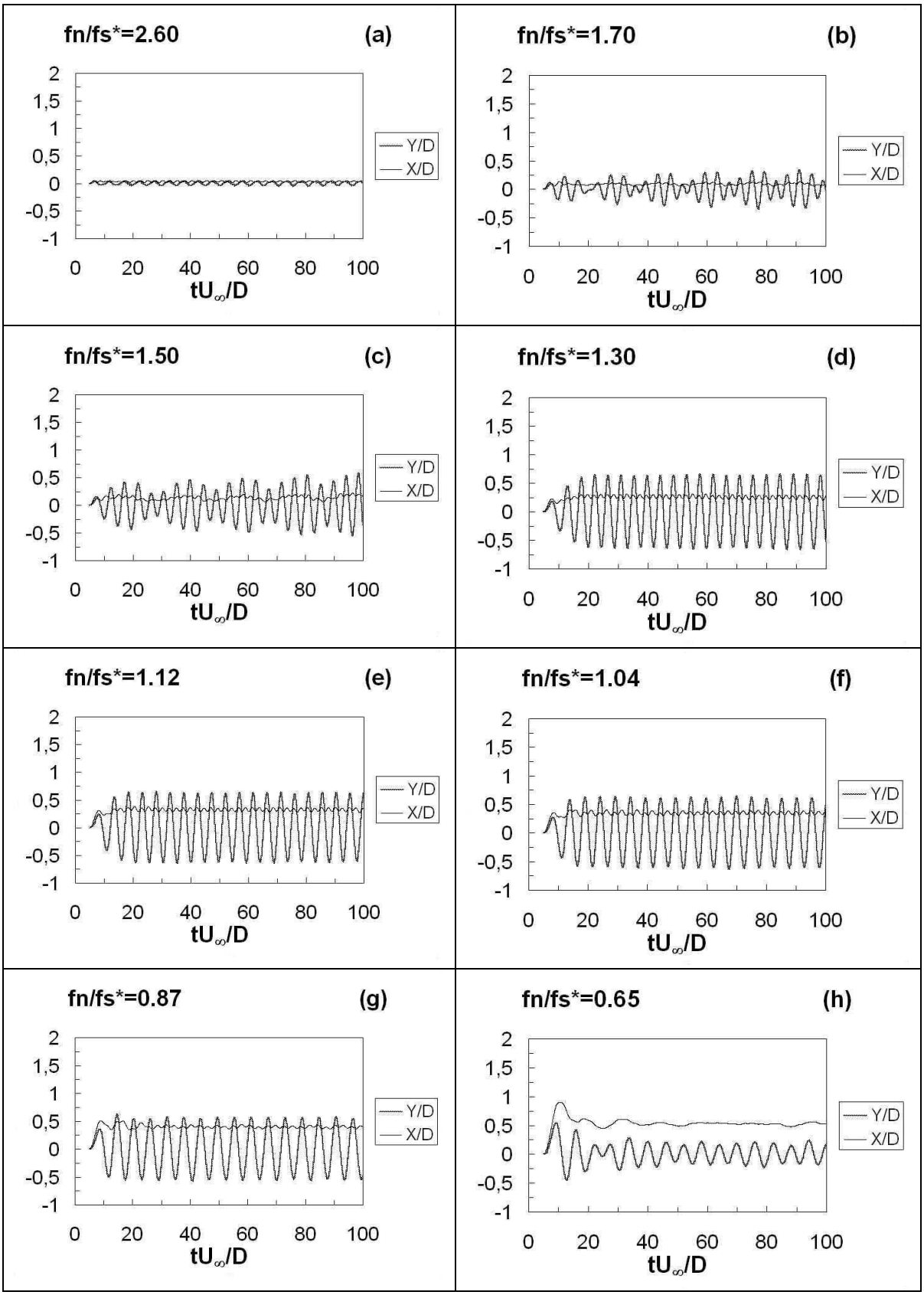


**Figure B3.2 Time histories of Displacements with various $f_n/f_s$* ratios for the case Sg=0.01 and M*=2**

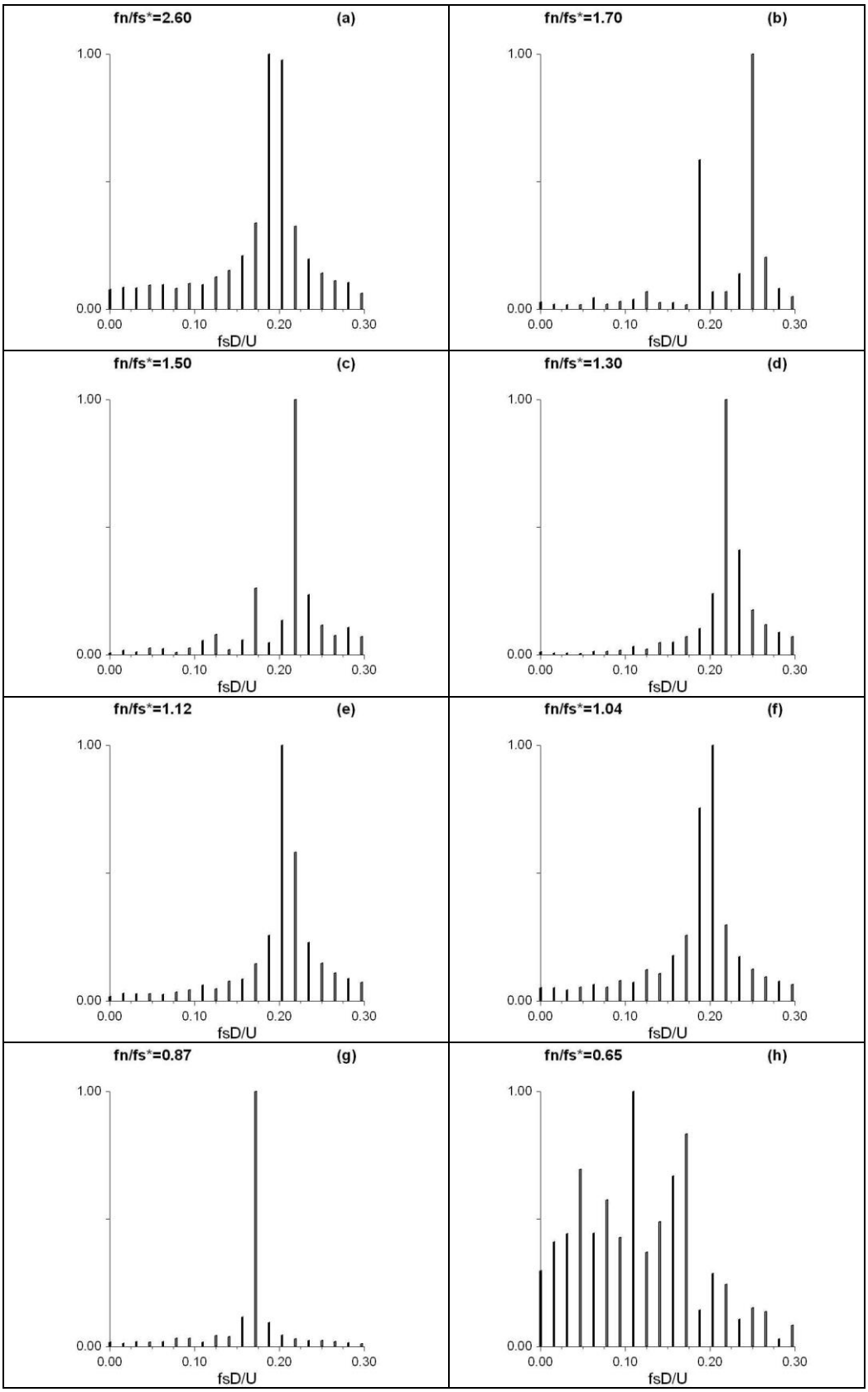


**Figure B3.3 Power Spectrum of $C_L$ oscillations with various $f_n/f_s$* ratios for the case Sg=0.01 and M*=2**

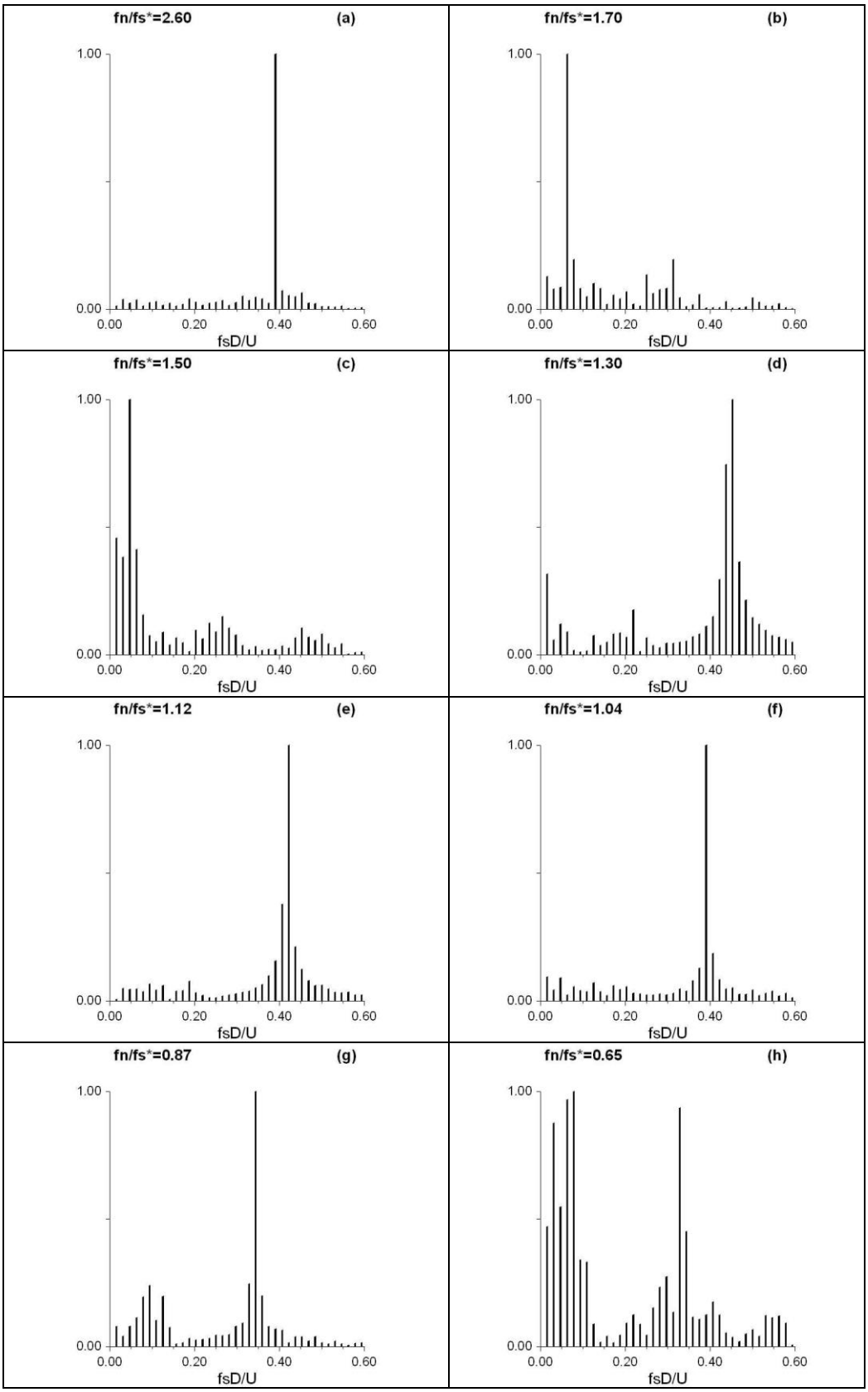


**Figure B3.4 Power Spectrum of $C_D$ oscillations with various $f_n/f_s$* ratios for the case Sg=0.01 and M*=2**

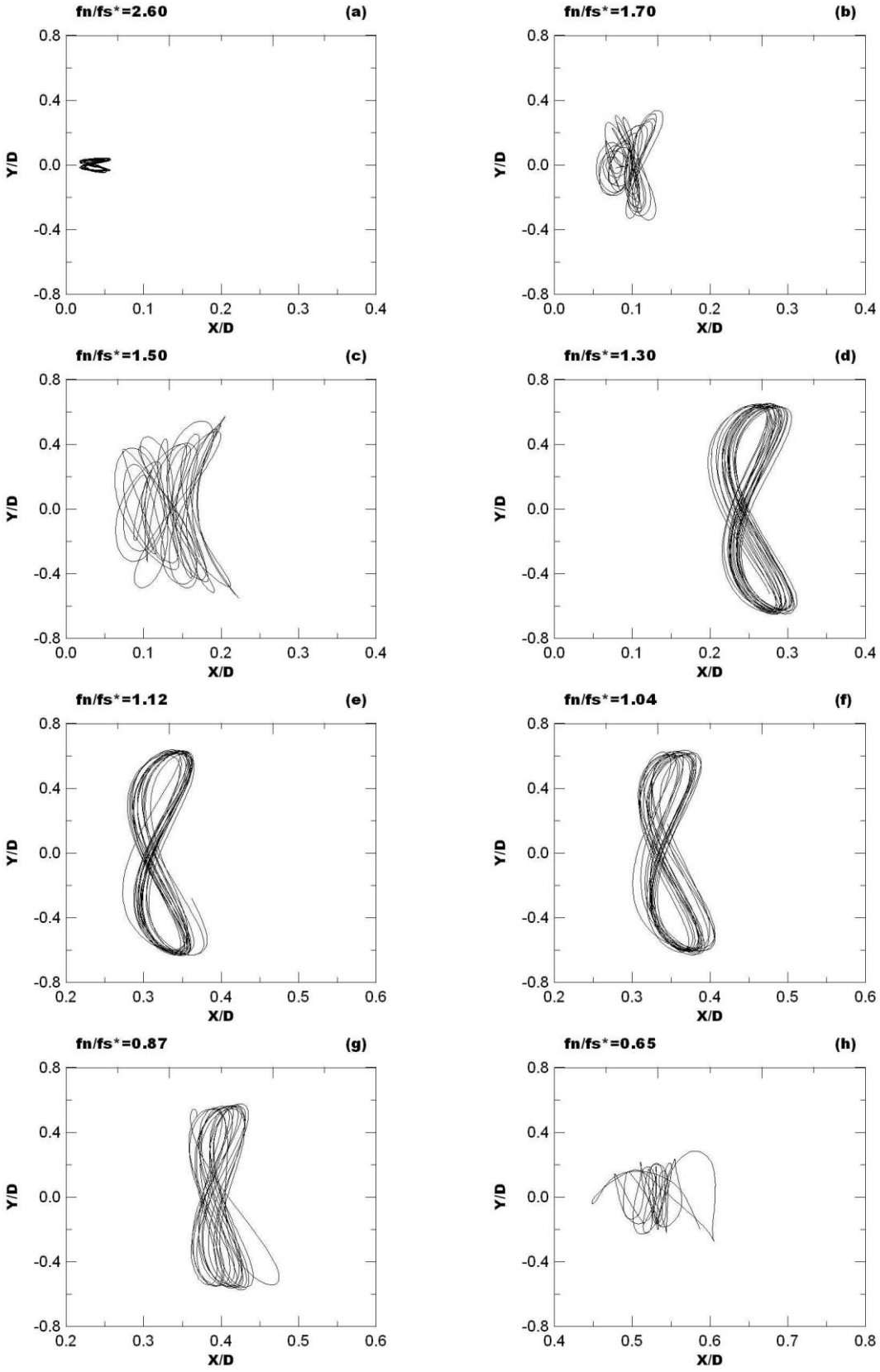


**Figure B3.5 Displacement Phase plots with various $f_n/f_s$* ratios for the case with Sg=0.01 and M*=2**

**APPENDIX B4**

**TIME HISTORIES OF LIFT COEFFICIENT, DRAG COEFFICIENT, TRANSVERSE OSCILLATION AND STREAMWISE OSCILLATION, POWER SPECTRUM OF LIFT AND DRAG COEFFICIENTS, DISPLACEMENT PHASE PLOT FOR THE CASE M*=3, Sg=0.01**

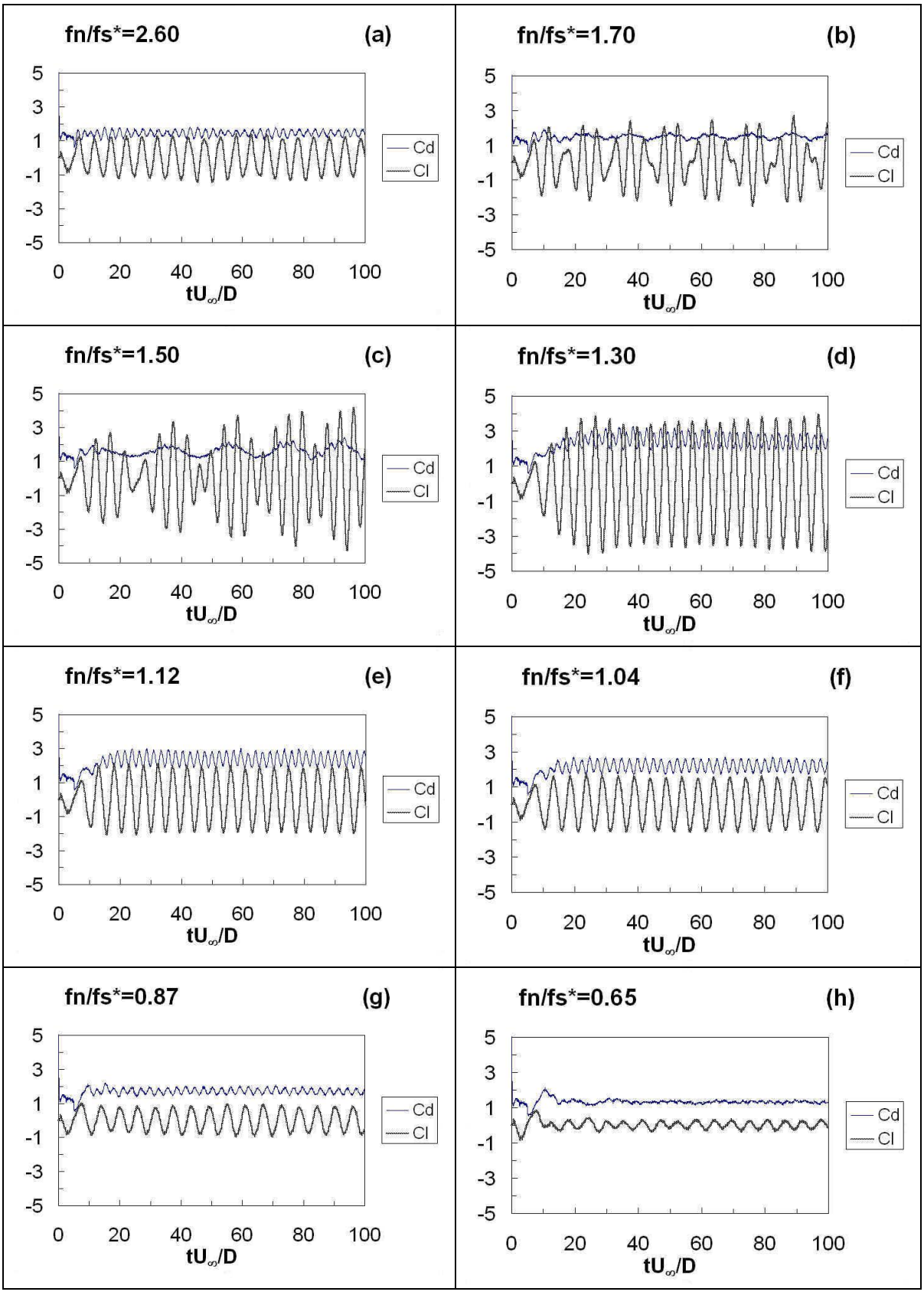


**Figure B4.1 Time histories of $C_D$ and $C_L$ coefficients with various $f_n/f_s$* ratios for the case Sg=0.01 and M*=3**

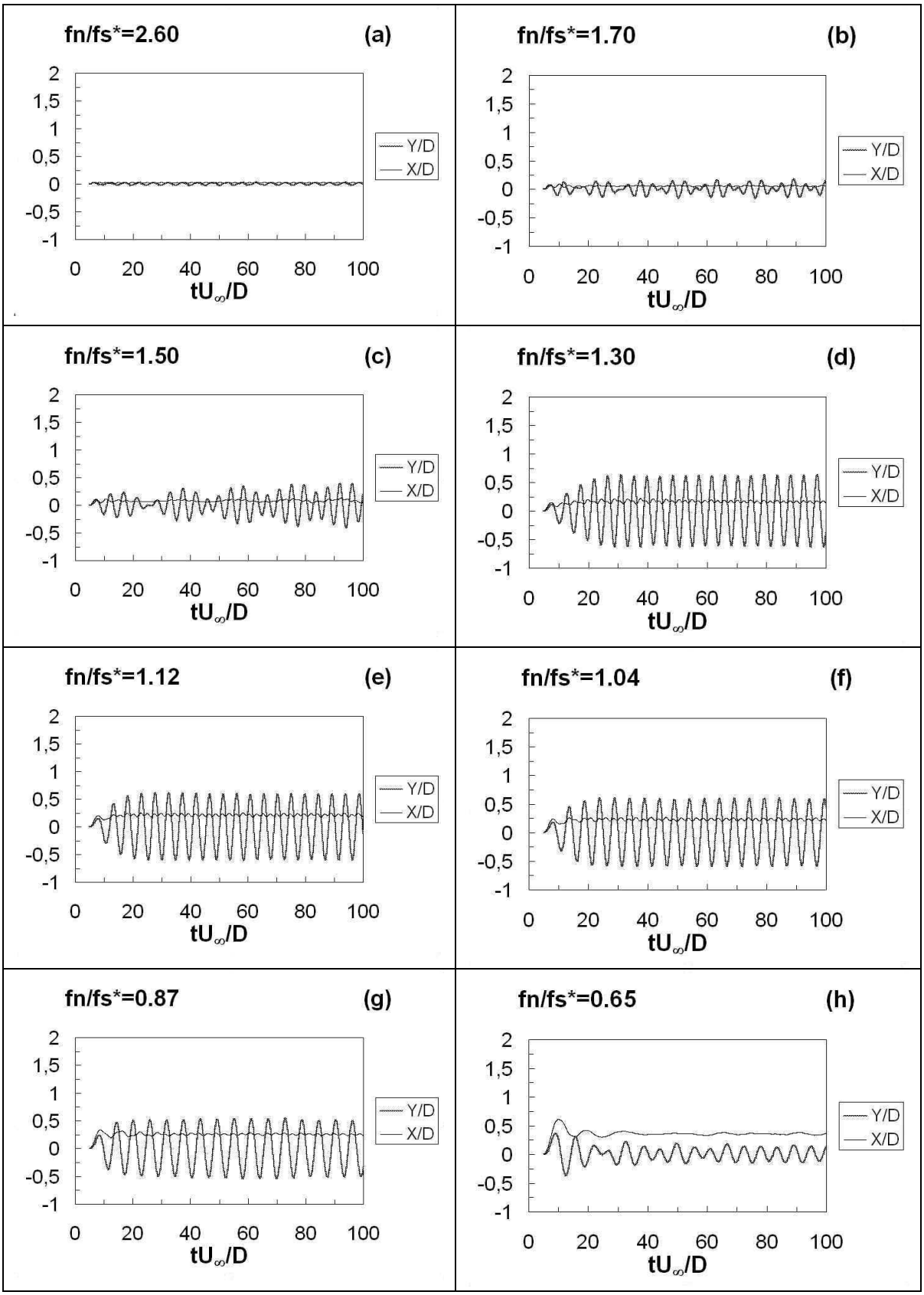


**Figure B4.2 Time histories of Displacements with various $f_n/f_s$* ratios for the case Sg=0.01 and M*=3**

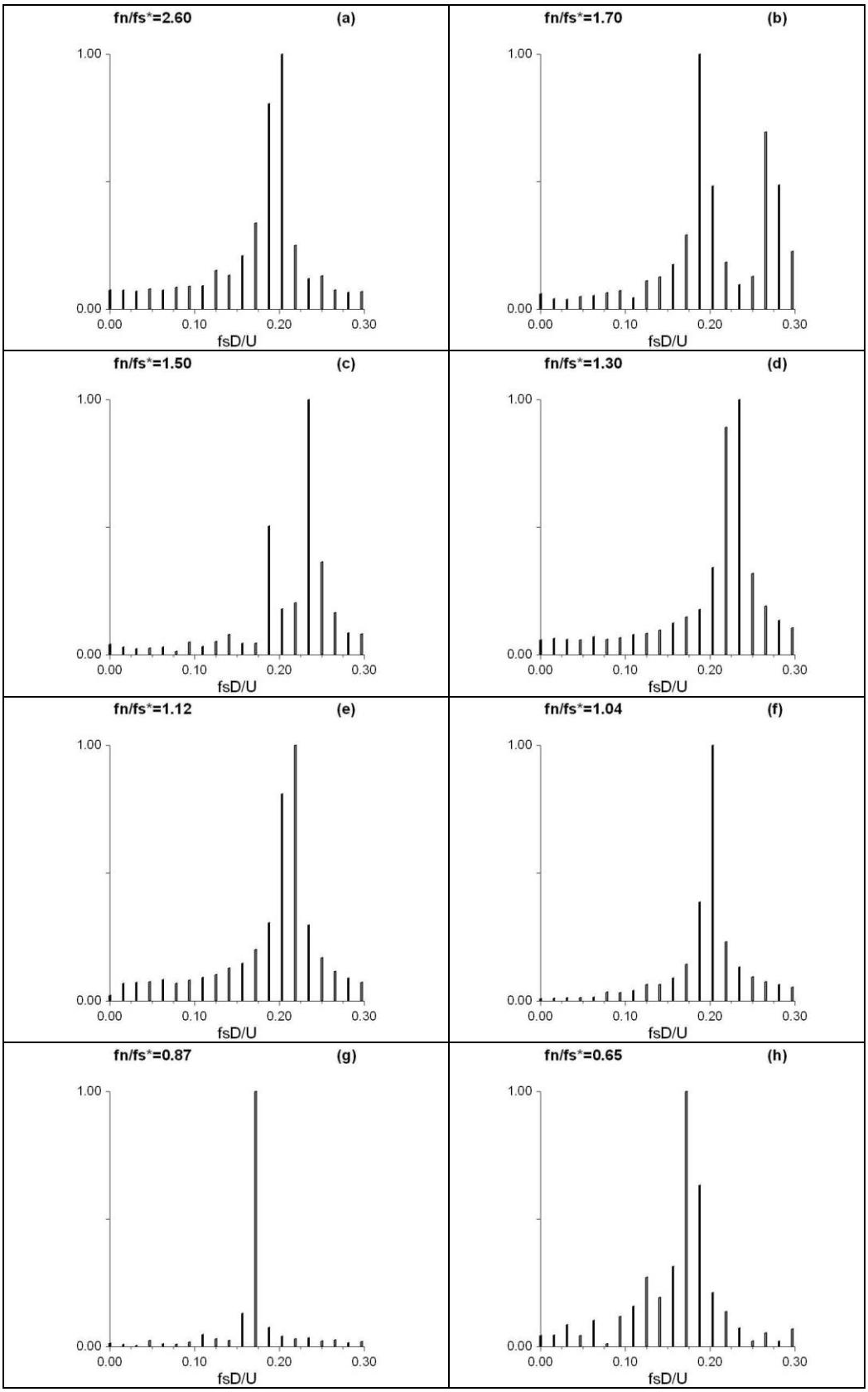


**Figure B4.3 Power Spectrum of $C_L$ oscillations with various $f_n/f_s$* ratios for the case Sg=0.01 and M*=3**

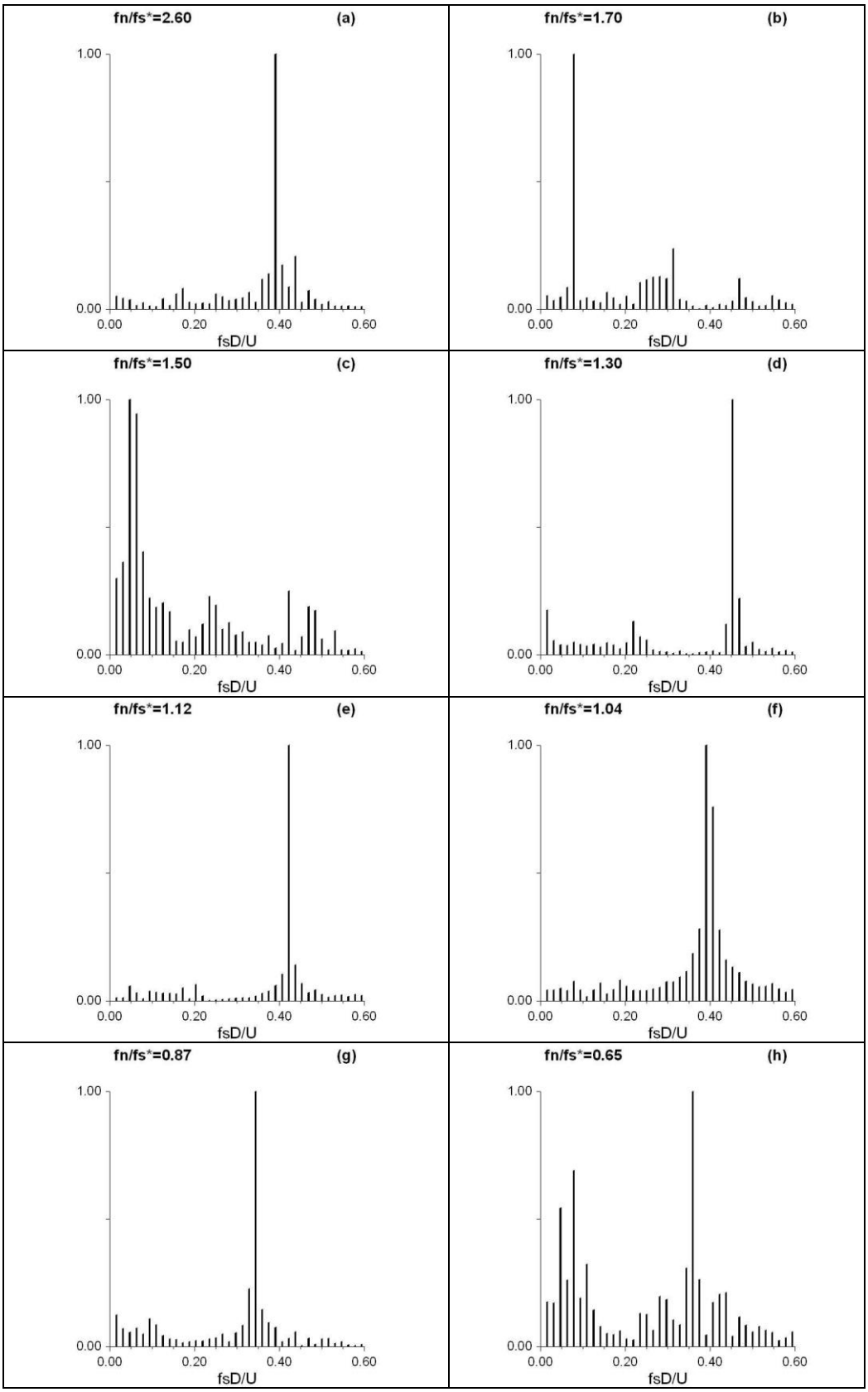


**Figure B4.4 Power Spectrum of $C_D$ oscillations with various $f_n/f_s$* ratios for the case Sg=0.01 and M*=3**

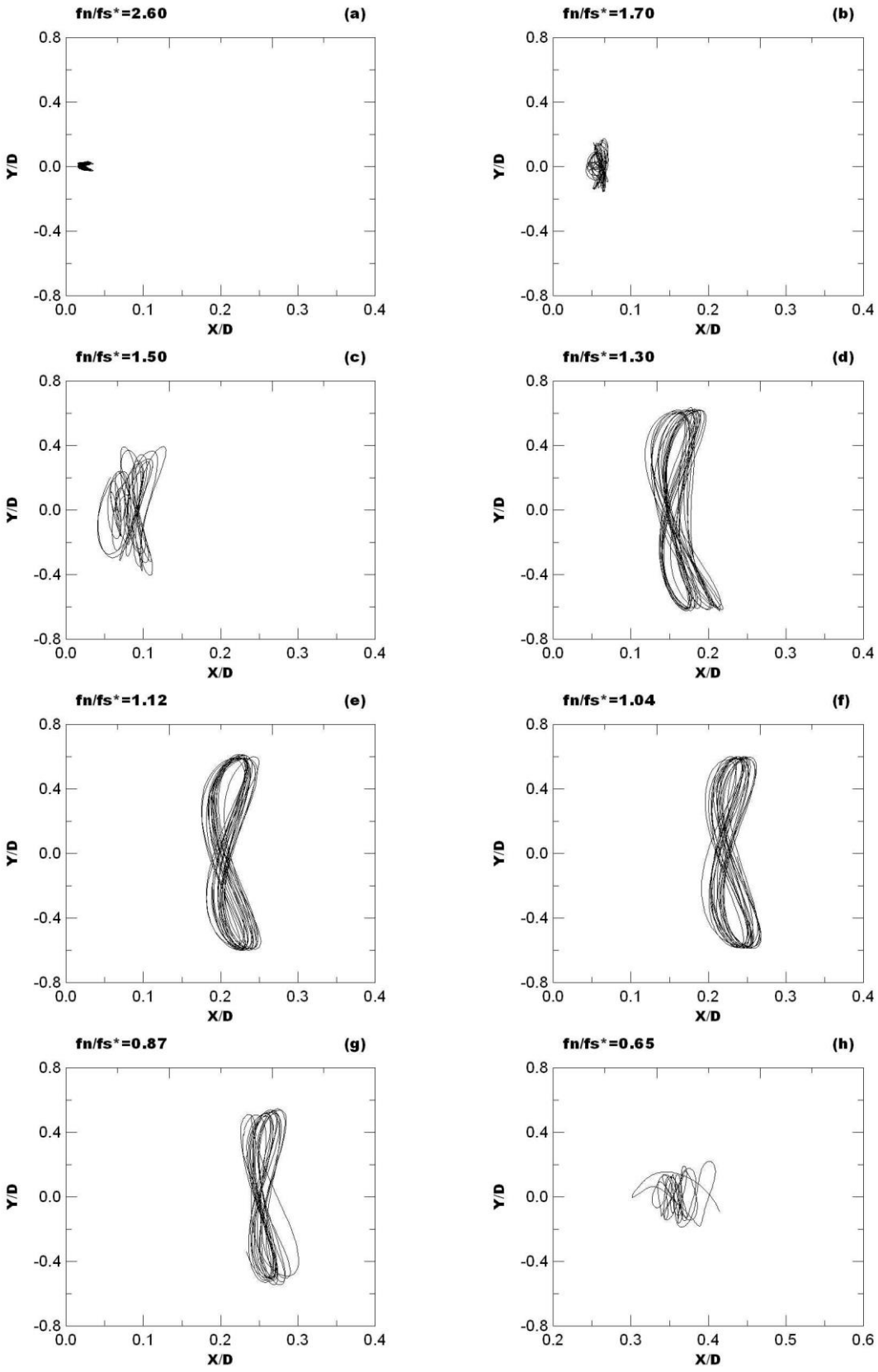


**Figure B4.5 Displacement Phase plots with various $f_n/f_s$* ratios for the case with Sg=0.01 and M*=3**

**APPENDIX B5**

**TIME HISTORIES OF LIFT COEFFICIENT, DRAG COEFFICIENT, TRANSVERSE OSCILLATION AND STREAMWISE OSCILLATION, POWER SPECTRUM OF LIFT AND DRAG COEFFICIENTS, DISPLACEMENT PHASE PLOT FOR THE CASE M*=10, Sg=0.01**

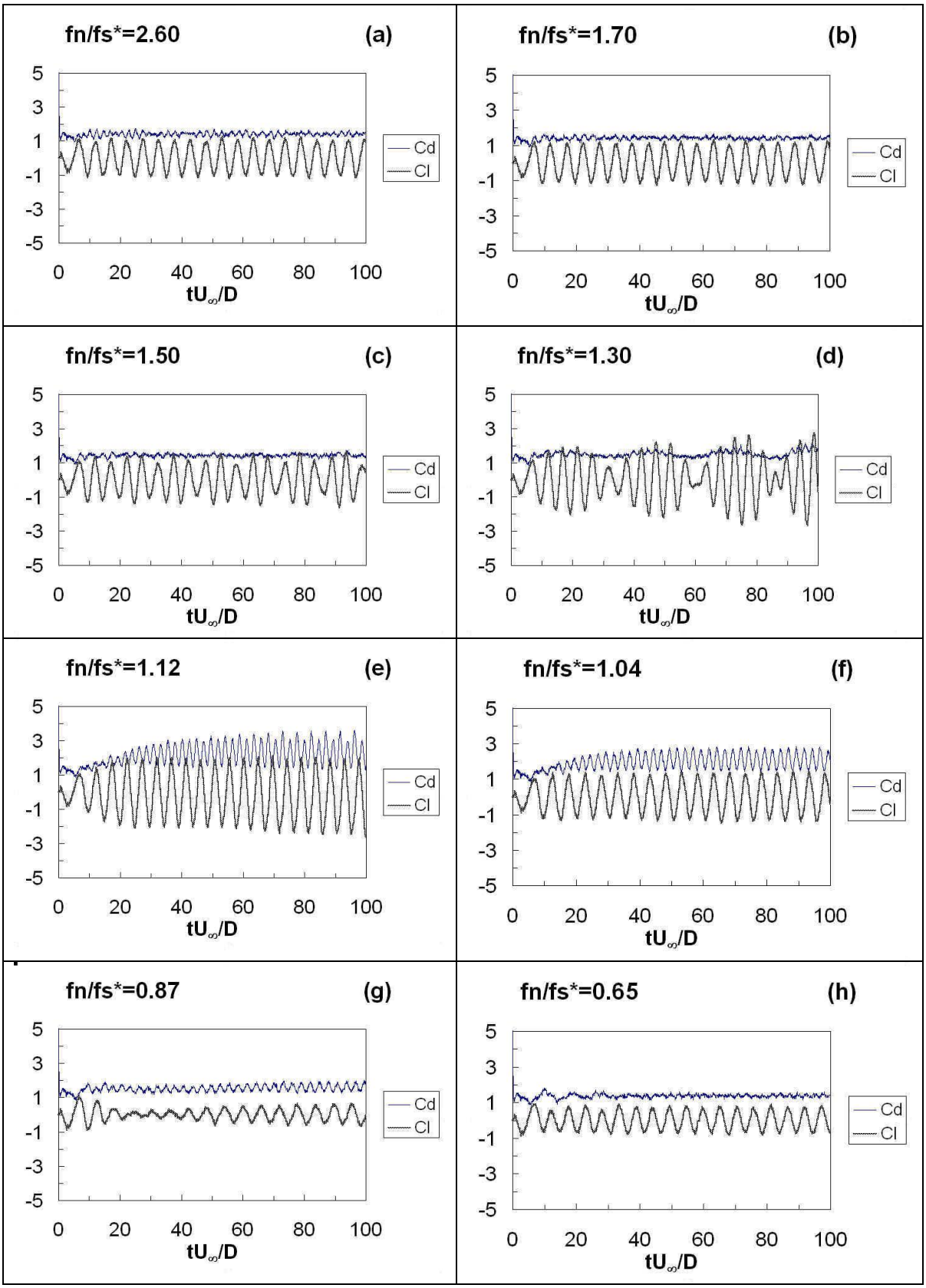


**Figure B5.1 Time histories of $C_D$ and $C_L$ coefficients with various $f_n/f_s$* ratios for the case Sg=0.01 and M*=10**

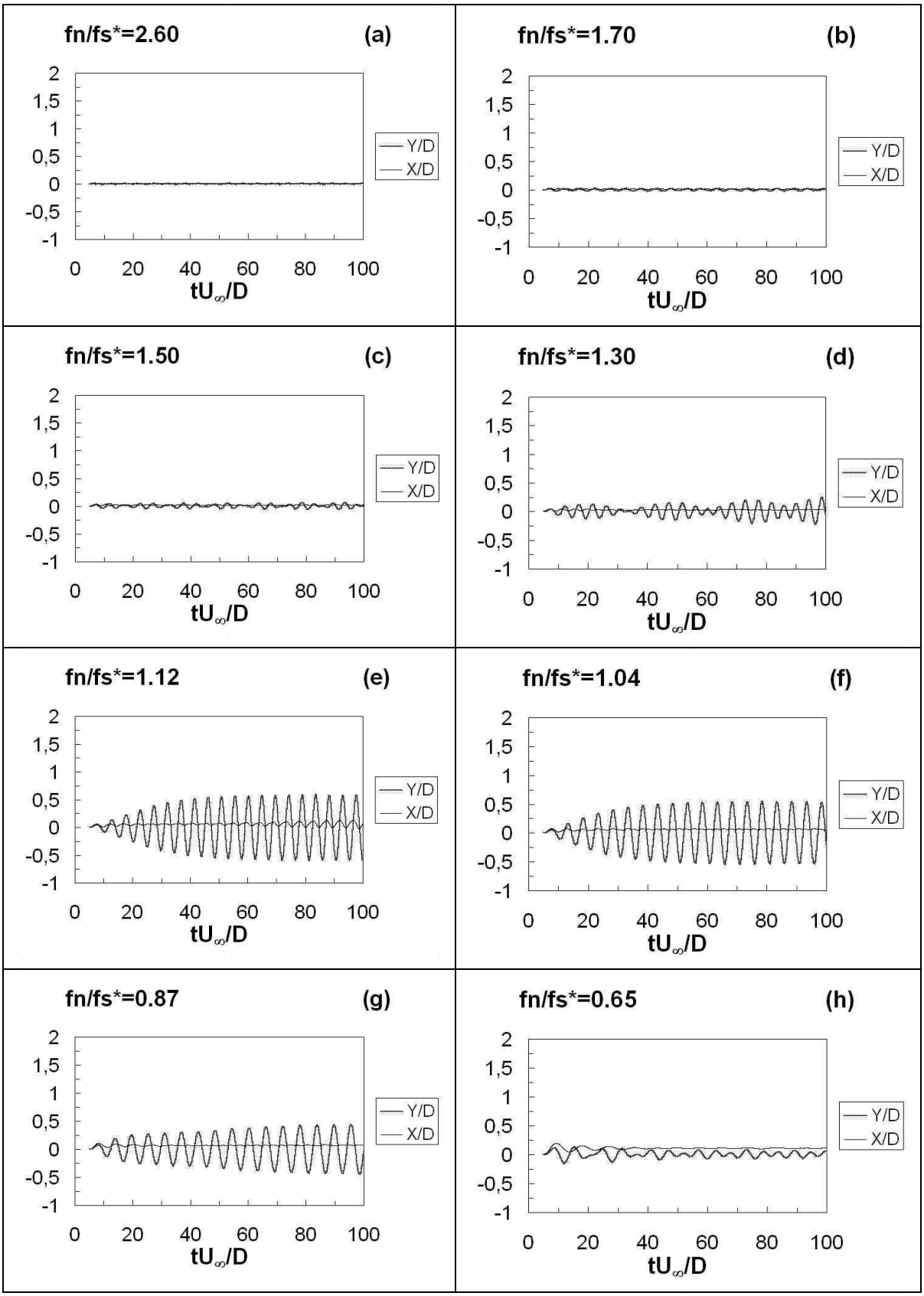


**Figure B5.2 Time histories of Displacements with various $f_n/f_s$* ratios for the case Sg=0.01 and M*=10**

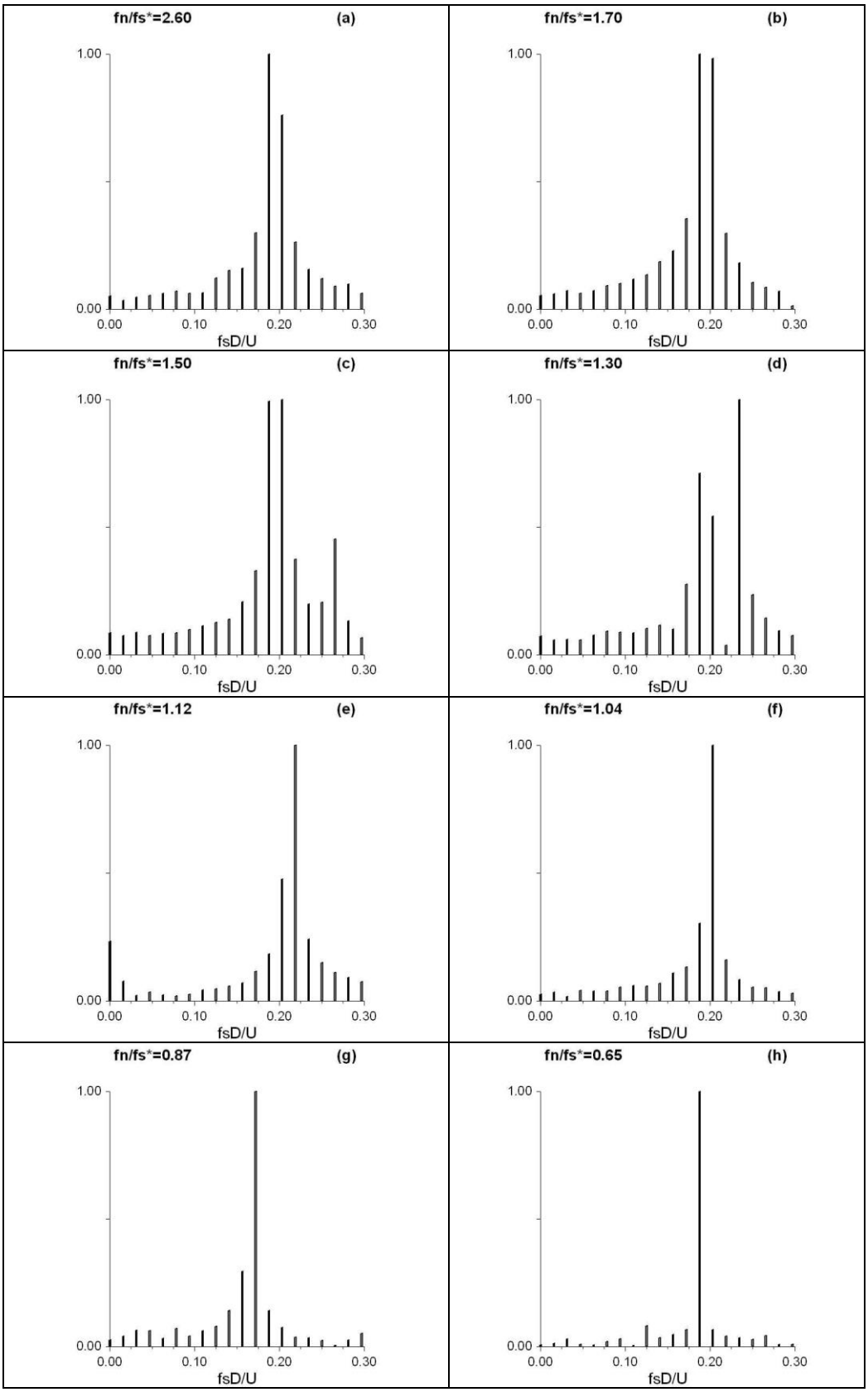


**Figure B5.3 Power Spectrum of $C_L$ oscillations with various $f_n/f_s$* ratios for the case Sg=0.01 and M*=10**

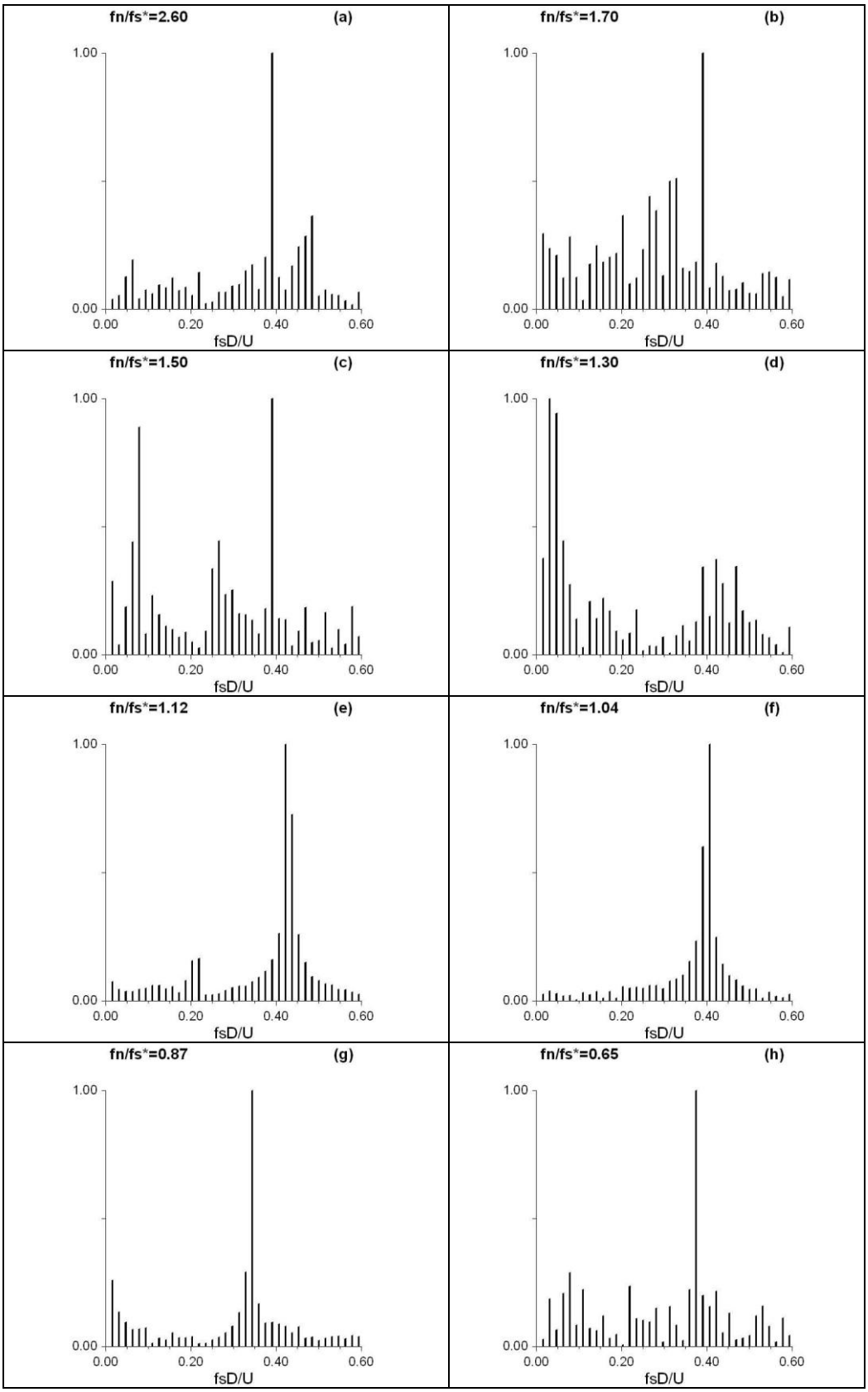


**Figure B5.4 Power Spectrum of $C_D$ oscillations with various $f_n/f_s$* ratios for the case Sg=0.01 and M*=10**

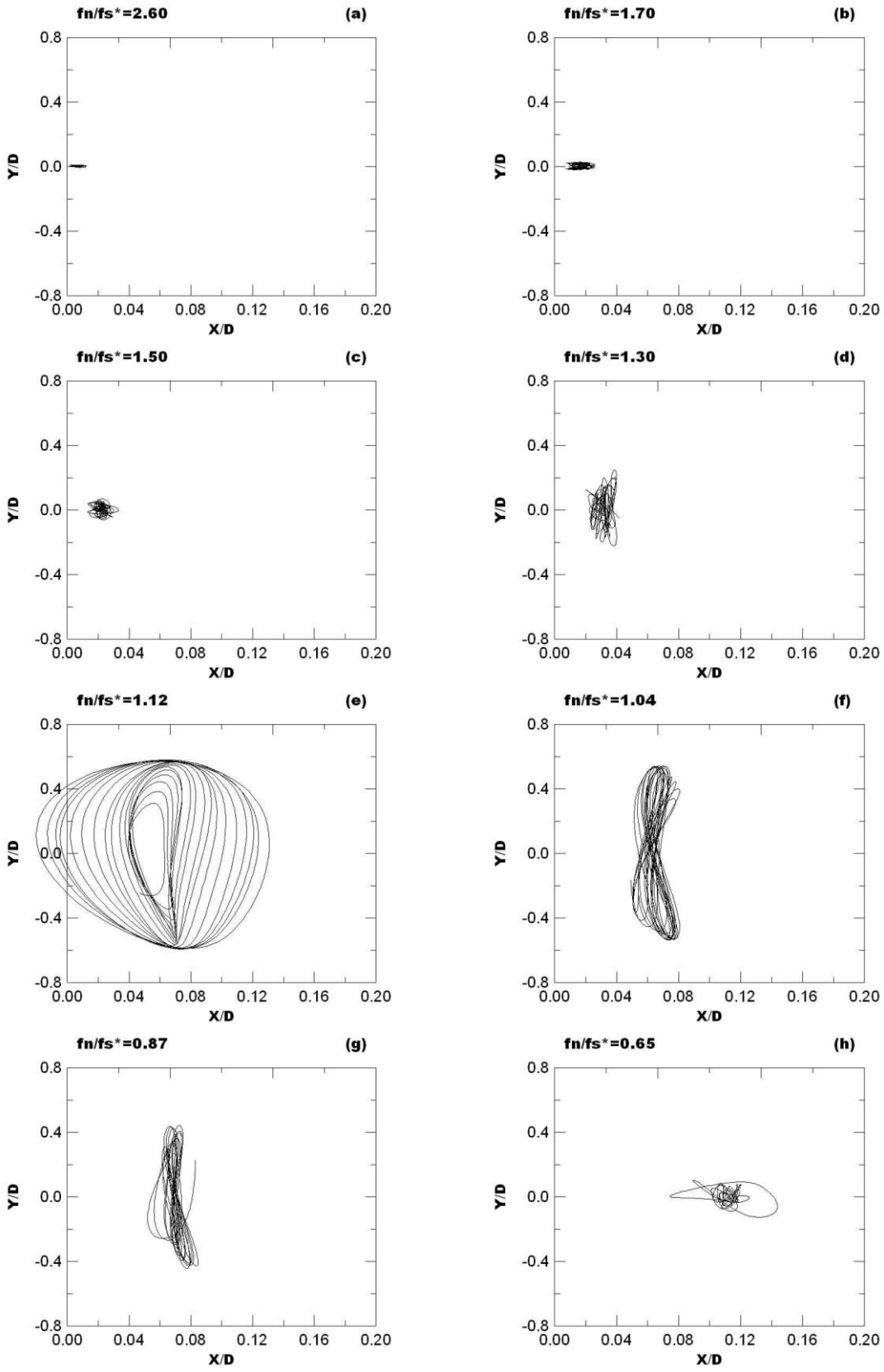


**Figure B5.5 Displacement Phase plots with various $f_n/f_s$* ratios for the case with Sg=0.01 and M*=10**

**BIOGRAPHY**

Salim KOÇ was born in Kırşehir in 1977. He graduated from the Anatolian High School of Malatya in 1995. He obtained his BSc. degree from I.T.U., Department of Aeronautical Engineering. He started his graduate education in I.T.U., Institute of Science and Technology, Aeronautical Engineering Department in 1999. He has been working in I.T.U., Faculty of Aeronautics and Astronautics as a research assistant since 2000.